Spring 2023

A Network of Low-Cost Multi-Pollutant Air Quality Sensors for Evaluating Fine-Scale Exposure Disparity in Twin Cities, MN

P M Varuni Abhayaratne
Missouri University of Science and Technology

Department:

A NETWORK OF LOW-COST MULTI-POLLUTANT AIR QUALITY SENSORS FOR EVALUATING FINE-SCALE EXPOSURE DISPARITY IN TWIN CITIES, MN

by

PANIK MUDIYANSELAGE VARUNI K. ABHAYARATNE

A THESIS

Presented to the Graduate Faculty of the

MISSOURI UNIVERSITY OF SCIENCE AND TECHNOLOGY

In Partial Fulfillment of the Requirements for the Degree

MASTER OF SCIENCE IN ENVIRONMENTAL ENGINEERING

2023

Approved by:

Dr. Yang Wang, Advisor
Dr. Jiayu Li
Dr. Sanjay Madria

ABSTRACT

Poor air quality is detrimental to health and is a leading environmental risk factor for early death globally. The massive scale of urbanization and population growth has led urban air quality to become a global concern as the release of air pollutants into the atmosphere continues to increase. Air quality has traditionally been monitored using reference-grade monitoring stations that are expensive and sparsely distributed. Low-cost sensors can complement existing regulatory networks to provide more spatial detail, capturing fine-scale variations. This study investigates spatiotemporal pollutant patterns, exposure disparities and environmental justice using data collected from a two-year (2019-2021) deployment of a multi-pollutant ($PM_{2.5}$, CO, O_3, NO_2, NO, SO_2, PM_{10}) low-cost sensor network located in the Minneapolis-St Paul metropolitan area. The study focuses on 45 sensors in the network to identify fine-scale spatial variations within an urban region. This study uses several data analysis techniques to investigate the spatiotemporal variability of pollutant concentrations across Twin Cities, MN. Measurement of air quality at a fine-scale can provide insight to pollution hot spots and transient peaks and help improve efforts to protect the health of vulnerable populations. The analyses conducted demonstrate the utility of a dense air quality sensor network and the techniques used can easily be replicated for low-cost networks located elsewhere.

ACKNOWLEDGMENTS

I am grateful for all that have contributed in some way to make the work described in thesis possible. To Dr. Yang Wang, my academic advisor: thank you for accepting me into your group, for your time, insight, guidance, patience and endless encouragement throughout this process. You have been an incredible mentor. I would like to thank Dr. Monika Vadali, the project manager of the Assessing Urban Air Quality project at the Minnesota Pollution Control Agency (MPCA) for making this study possible. I gratefully acknowledge Dr. Jiayu Li for making the collaboration with MPCA possible and for the constructive feedback offered during this research. I would also like to thank Dr. Jiayu Li and Dr. Sanjay Madria for taking time out of their busy schedules to serve on my MS thesis committee and for their interest in my work. To Ms. Jody Seely and Ms. Jeannie Werner: I am thankful for all the support. You make this department a welcoming place. I would like to acknowledge the professors at the Civil, Architectural and Environmental Engineering Department. My graduate experience benefitted greatly from the courses taken and the opportunities provided. Finally, to my loving parents and my wonderful husband: I am grateful in more ways than I can express for your unconditional love and support. I dedicate this thesis to you.

TABLE OF CONTENTS

Page

LIST OF FIGURES

Page

LIST OF TABLES

Page

1. INTRODUCTION

Poor air quality is detrimental to health and is a leading environmental risk factor for early death globally (State of Global Air Report, 2020). According to the World Health Organization, approximately seven million premature deaths attributable to air pollution occur each year worldwide (WHO). The massive scale of urbanization and population growth which has resulted in increase of traffic, industrialization and energy use has led urban air quality to become a global concern as the release of air pollutants into the atmosphere continues to increase (Kumar et al., 2014).

In the United States, air quality has traditionally been monitored using stations equipped with Federal Reference Method (FRM) or Federal Equivalent Method (FEM) instruments. These traditional networks produce high quality data as the FRM and FEM designation for instruments is established through a strict testing protocol (Jiao et al., 2016). However, the typical purchase cost of these reference monitors ranges from $15,000 to $40000 (USD) and their operation costs are high due to the need for shelter to house the instrumentation, the need for highly trained technical staff, maintenance, repair and quality assurance (US EPA, 2019). As a result, existing networks consist of only a limited number of monitoring sites within an urban environment. Field studies (Jiao et al., 2016; Tanzer et al., 2019) have shown that there are fine-scale spatial variations in outdoor air quality due to localized impacts of source emissions and traditional networks are too sparse to capture these variations.

Owing to recent advances in sensor technology, traditional networks can now be supplemented using lower-cost air quality monitors to enhance spatial coverage. As

reported by US EPA (2019), the typical purchase cost of a low-cost sensor is in the range of $200 to $5000 (USD), a fraction of the price of a reference monitor. The lower cost as well as greater flexibility in where they can be installed, makes it possible to capture fine-scale spatial variations within an urban area, as low cost sensors can be deployed at higher density and can provide more spatial detail than traditional air quality monitoring stations (Schneider, 2018).

This study presents results from a two-year deployment of a low-cost sensor network in Twin Cities, MN, USA, focusing on 45 sensors in the network to identify fine-scale spatial variations within an urban region. Within this study, “fine-scale” is defined as variations among US ZIP codes throughout the Minneapolis-St Paul metropolitan area. The objective of this study is to use this widespread network of low-cost air quality monitors, to investigate disparities in air pollution exposure and environmental justice within the Twin Cities region.

Environmental justice is the fair treatment and meaningful involvement of all people regardless of race, color, national origin, or income, with respect to the development, implementation, and enforcement of environmental laws, regulations, and policies (US EPA). Previous research shows that the health burden of air pollution is not evenly shared and that certain populations such as those residing in low income communities and communities of color in the United States are exposed to higher-than-average levels of air pollution (Liu et al., 2021). In this study, a network of low cost sensors is used to investigate exposure disparities across income groups in the city-scale (Twin Cities, MN) and whether vulnerable populations are disproportionately impacted by specific air pollutants. This dense network of air quality monitors is used to investigate

whether low income sites do in fact have higher concentrations of specific EPA criteria air pollutants in comparison to sites with higher income. Studies have found associations between redlining— a racially discriminatory housing policy that was outlawed in 1968— and present-day environmental health disparities in the United States (Lane et al., 2022). As reported by Lane et al. (2022), there is limited research on air pollution exposure and redlining. In this study, the network of low-cost sensors in urban Minnesota is also used to explore associations between Home Owners' Loan Corporation (HOLC) grade and air pollution disparities in the Twin Cities.

It is noteworthy to mention that this study is observational and examines associations between socioeconomic factors and air pollutant concentration levels and is not designed to distinguish causation. It is also important to note that, currently, low-cost sensors cannot replace traditional monitors for regulatory monitoring or personal exposure quantification. However, this study demonstrates the potential of low-cost sensor networks to complement existing regulatory networks to understand air quality variability at a fine spatial scale.

2. MATERIALS AND METHODS

2.1. SENSOR NETWORK

Figure 2.1 Map of sensor sites.

This study focuses on data from 45 air quality monitors that were deployed throughout Minneapolis-St Paul (Figure 2.1) over June 2019- June 2021, under the Assessing Urban Air Quality Project conducted by the Minnesota Pollution Control Agency (MPCA). The Assessing Urban Air Quality Project aims to understand small-scale variability of harmful air pollutants within densely populated regions and the sensor network has at least one monitoring unit in each ZIP code in the Twin Cities, with multiple

monitoring sites in ZIP codes that cover a larger area. The network consists of AQMesh pods and each monitoring unit reports data for particulate matter (PM_{10}, $PM_{2.5}$, and PM_1), carbon monoxide (CO), ozone (O_3), nitrogen dioxide (NO_2), nitric oxide (NO), and sulfur dioxide (SO_2) and the sensors are able to obtain a reading every minute to provide the average pollutant concentration for each hour. AQMesh air quality monitoring systems have demonstrated reliability and performance through global co-location comparison trials against calibrated reference stations (Randle, 2016).

2.2. SENSOR DATA ANALYSIS

2.2.1. Time Variation Plots of Concentration. To assess sensor performance seasonal and diurnal trends were generated using data from all 45 sensor locations over the years 2019-2021. Median pollutant concentrations were considered instead of the mean to avoid influence of extreme outlier values. To explore monthly patterns over 2019-2021, hourly air pollutant concentration data were assigned into half-month bins and a median concentration was obtained for each bin. The objective of using 15-day median concentrations was to observe monthly trends more closely. To observe daily trends for each of the pollutants during 2019-2021, concentration data were binned into each hour of the day and a median value was obtained for each bin. In addition to the median values, q1 (25th percentile) and q3 (75th percentile) were also plotted to obtain a general idea on the distribution of pollutant concentrations.

2.2.2. Coefficient of Divergence (COD). Coefficient of Divergence (COD) was computed to evaluate the significance of concentration differences among sensor sites (Krudysz et al., 2008; Tanzer et al., 2019). The COD was computed using equation (1)

(Tanzer et al., 2019). COD values range from 0 to 1; 0 indicating similar concentrations and 1 indicating extreme concentration differences among a sensor pair (Pakbin et al., 2010). COD values greater than 0.2 were considered to be indicative of significant spatial heterogeneity on an hourly basis (Krudysz et al., 2008; Tanzer et al., 2019). Due to data incompleteness, only the measurements from the year 2020 were considered and only the sensor sites having readings for every hour of 2020 have been included in the analysis.

$$COD = \sqrt{\frac{1}{N}\sum_{i=1}^{N}\left(\frac{x_{iA}-x_{iB}}{x_{iA}+x_{iB}}\right)^2} \qquad (1)$$

Where,

N: number of paired observations

i :time period (each hour)

x_{iA}: hourly pollutant concentration measured at site A

$x_{iB:}$ hourly pollutant concentration measured at site B

2.2.3. Power Spectral Analysis. To identify significant periodicities within the time series of air quality data, the spectral density was estimated for each frequency using the mvspec package in R. To smooth the data, a Hann window was applied (Marinescu et al., 2019) considering frequency resolution, amplitude resolution and leakage reduction. Median values were calculated for each hour of the day for the entire dataset (45 sites). Frequencies with the highest spectral densities were identified as significant periodicities in the time series. When conducting the spectral analysis, data over the years 2019-2021 were separated into seasons. Throughout this paper, seasons are defined as follows: winter (December- February), spring (March- May), summer (June-August), and fall (September-

November) and accordingly, the dataset was categorized into eight subsets as summer 2019 (SM19), fall 2019 (FL19), winter 2019 (WN19), spring 2020 (SP20), summer 2020 (SM20), fall 2020 (FL20), winter 2020 (WN20) and spring 2021 (SP21) and the dominant periodicity of each subset was identified for all seven pollutants.

2.2.4. Exposure Based on Socioeconomic Disparities. Air quality disparities in relation to level of income were explored among ZIP codes in the Minneapolis-St Paul area. Per capita income and percent population below poverty line were used as indicators of socioeconomic status to evaluate variability across income groups. Income statistics data were obtained from the US Census Bureau's American Community Survey. The sensor locations were sorted from highest to lowest per capita income ($78295 to $3998) and the top five sites (namely, City of Lakes Building, Cedar-Isles-Dean, Kenny, MPCA office and Highland Park Middle School) and bottom five sites (namely, Harding High School, Jackson Elementary School, Hawthorne, Jordan and Bruce Vento Elementary School) were identified. It is important to note that sites with missing data and anomalous data were eliminated during the process of sorting and selecting the top/bottom five sites. After the selecting the five sites of highest per capita income, the three sites having the lowest percent population below poverty line were identified as “high income” sites in this study. Similarly, among the five sites of lowest per capita income, the three sites having the highest percent population below poverty line were defined as “low income” sites.

By obtaining Pearson correlation coefficients (r), the association between pollutant concentration and income variables were further investigated.

$$r_{xy} = \frac{1}{n-1}\sum_{i=1}^{n}\left(\frac{x_i-\bar{x}}{\sigma_x}\right)\left(\frac{y_i-\bar{y}}{\sigma_y}\right) \qquad (2)$$

Where,

n: sample size

x_i: x-variable value

$\bar{x}$: x-variable sample mean

y_i: y-variable value

$\bar{y}$: y-variable sample mean

σ_x: x-variable sample standard deviation

σ_y: y-variable sample standard deviation

All air pollutant observations were binned depending on the sensor location. Then, a median air pollutant concentration was calculated from each bin, representative of the average air quality at each sensor location. Per capita income of each sensor location (ZIP code) was selected as the desired income indicator. Finally, the Pearson correlation coefficient was calculated between these 45 observation pairs as a measure of their linear dependence. Furthermore, it was explored whether a correlation exists between percent reduction in median pollutant concentration over 2019-2021 and per capita income. Percent reduction in median air pollutant concentration was obtained as follows:

$$\% \text{ reduction in pollutant concentration} = \frac{M_{2021} - M_{2019}}{M_{2019}} \times 100 \qquad (3)$$

Where,

M_{2019}: median air pollutant concentration in 2019

M_{2021}: median air pollutant concentration in 2021

Delving deeper, a Simple Linear Regression (SLR) model was used to explore whether there is a statistically significant linear relationship between per capita income (explanatory) and median pollutant concentration/ percent reduction in median pollutant concentration (response).

$$y = \beta_0 + \beta_1 x + \varepsilon \qquad (4)$$

Where,

y: overall median pollutant concentration

or percent reduction in median pollutant concentration

x: per capita income

ε: random error

The non-parametric counterpart of an independent-means t-test, the Mann-Whitney U test (also known as the Wilcoxon Rank Sum Test), was used to examine whether there is a statistically significant difference between median pollutant levels among groups of high income and low income sites. In determining these groups, the median per capita income was calculated and this value was considered to be the point separating the income distribution into two groups as high income and low income (US Census Bureau). Accordingly, sites having income above the median were defined as high income sites and those having income below the median were identified as low income sites to conduct this test. Determination of the Mann-Whitney test statistic "U" involves the following equation:

$$U_1 = n_1 n_2 + \frac{n_1 (n_1 + 1)}{2} - R_1$$
$$U_2 = n_1 n_2 + \frac{n_2 (n_2 + 1)}{2} - R_2 \qquad (5)$$

Where,

n_1, n_2: sample size of group1 and group 2 respectively

R_1, R_2: sum of ranks for group 1 and group 2 respectively

2.2.5. Exposure Based on Historical Redlining Maps. In order to investigate the association between historical redlining and present day air pollutant concentrations, the 1930s HOLC maps developed by University of Richmond's Mapping Inequality Project were used to identify the HOLC grade assigned to mapped sensor sites in the studied network. Only a single site was found to belong to HOLC category A ("best") in the studied region. For this reason, this study only evaluates disparities between the three remaining HOLC grades: B ("still desirable") – 10 sites, C ("still declining) -15 sites, and D ("redlined")-7 sites. Sites that did not fall within the bounds of graded regions were excluded from analysis (11 sites). Box-whisker plots were generated to visualize variations in pollutant concentrations across groups B, C and D.

2.2.6. Conditional Bivariate Probability Function (CBPF). Bivariate polar plots are a useful graphical technique that can display the variation of pollutant concentration with both the wind speed and wind direction in polar coordinates (Uria-Tellaetxe and Carslaw, 2014).The basic Conditional Probability Function (CPF) statistic can show the probability of high pollutant concentrations occurring by wind direction and thereby help identify source directions that dominate high concentrations (Ashbaugh et al., 1985; Uria-Tellaetxe and Carslaw, 2014). The CPF is defined as follows (Ashbaugh et al., 1985; Uria-Tellaetxe and Carslaw, 2014):

$$CPF_{\Delta\Theta} = \frac{m_{\Delta\Theta} \mid c \geq x}{n_{\Delta\Theta}} \qquad (6)$$

Where,

m_{Θ}: number of samples in wind sector $\Delta\Theta$ having concentration (c) greater than or equal to a predetermined threshold value (x)

n_{Θ}: total number of samples from wind sector $\Delta\Theta$

The Conditional Bivariate Probability Function (CBPF)—a combination of CPF and bivariate polar plots—allows the use of a third variable; wind speed. It is defined as (Uria-Tellaetxe and Carslaw, 2014):

$$CBPF_{\Delta\Theta,\Delta u} = \frac{m_{\Delta\Theta,\Delta u \mid c \geq x}}{n_{\Delta\Theta,\Delta u}} \qquad (7)$$

Where,

$m_{\Delta\Theta,\,\Delta u}$: number of samples in wind sector $\Delta\Theta$ with wind speed interval Δu having concentration (c) greater than or equal to a predetermined threshold value (x)

$n_{\Delta\Theta,\,\Delta u}$: total number of samples from wind sector $\Delta\Theta$ and wind speed interval Δu

Therefore, the bivariate case of the CPF function is not only useful in detecting source regions but also characterizing sources as it offers information on wind speed dependencies of concentrations (Uria-Tellaetxe and Carslaw, 2014). The polarPlot function in the openair R package was used to generate CBPF plots for a 75th percentile threshold. For wind speed (ws) and wind direction (wd) information, NCAR's CISL Research Data Archive was used and data for the Minneapolis−Saint Paul International

Airport station in the year 2020 were obtained. Sensor sites having data for every hour of the year were selected for analysis and the ws, wd data was used universally for all selected sensor sites. CBPF plots have been generated for spring 2020 (SP20), summer 2020(SM20), fall 2020(FL20) and winter 2020 (WN20) to observe seasonal variation.

3. RESULTS AND DISCUSSION

3.1. SEASONAL VARIABILITY

Figure 3.1, (a) through (g) illustrates the monthly trends of each pollutant for the years 2019 (blue), 2020 (purple) and 2021(green). Seasons are defined as follows: winter (December- February), spring (March- May), summer (June-August), and fall (September-November).

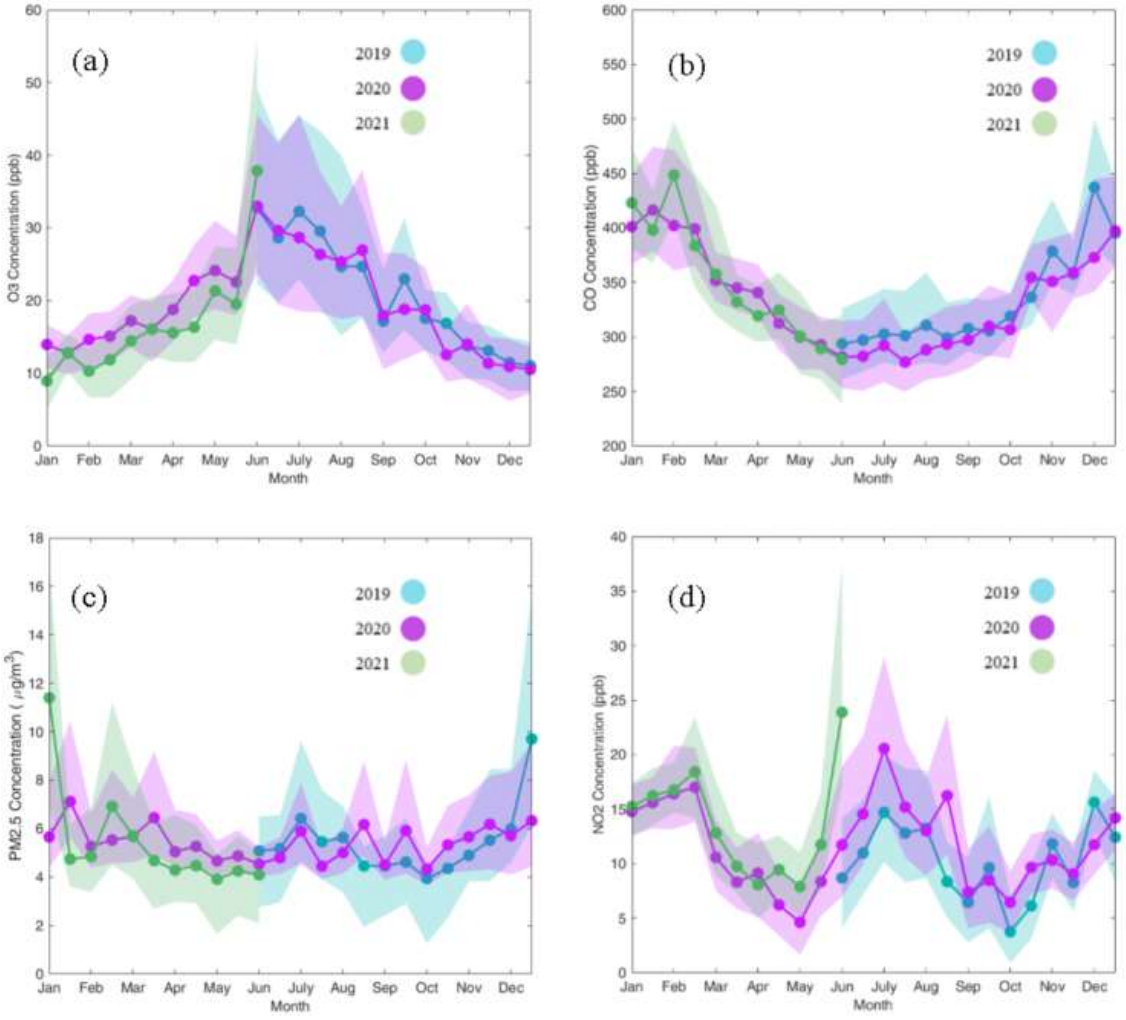

Figure 3.1 Monthly trends of overall network.

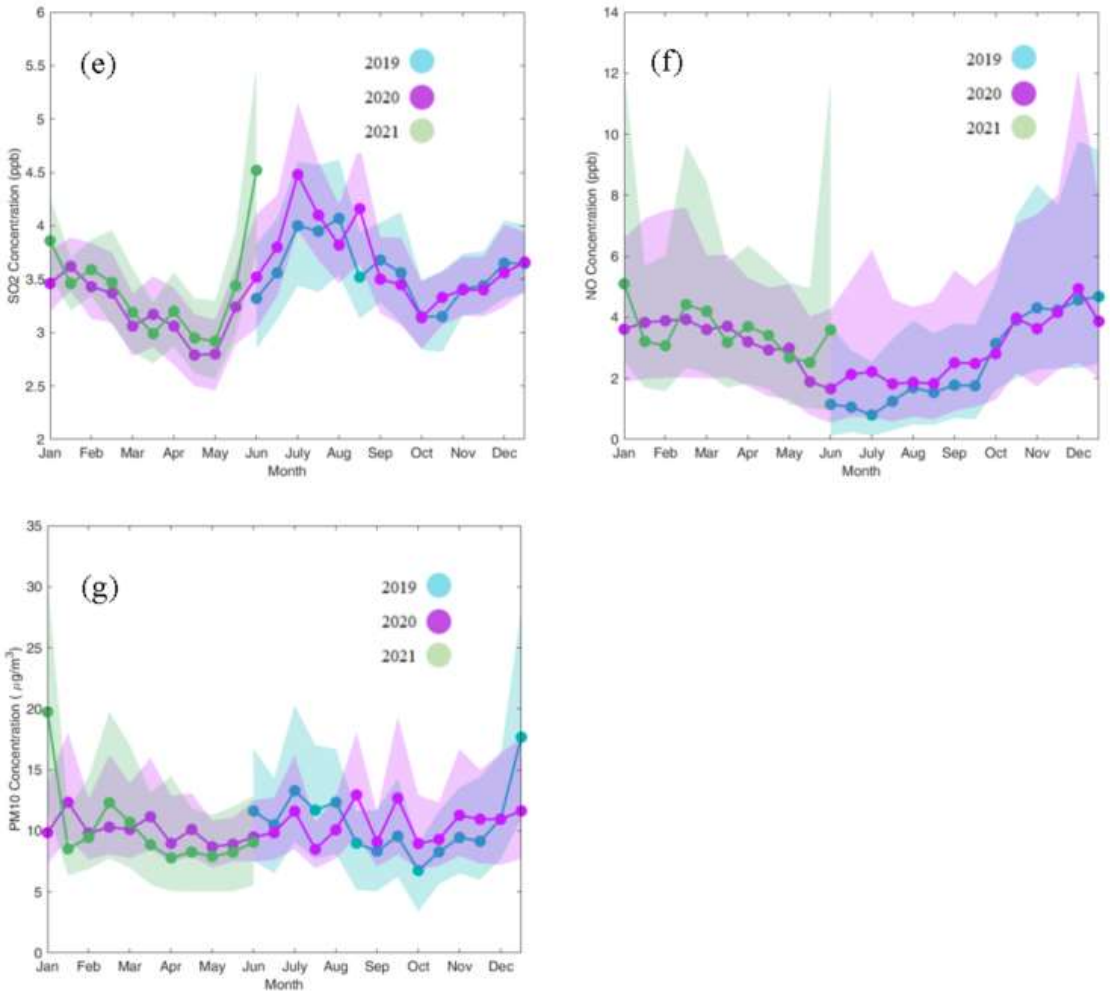

Figure 3.1 Monthly trends of overall network. (Cont.)

Results for CO (Figure 3.1(b)) indicate a high winter- low summer seasonality, with a highest median concentration of 450 ppb (winter 2020) and a lowest median concentration of 275 ppb (summer 2020). These seasonal differences may be attributed to winter heating, higher concentrations of hydroxyl (OH) radical and intense mixing processes during warmer months (Bi et al., 2022). It can be observed that both NO_2 (Figure 3.1(d)) and SO_2 (Figure 3.1(e)) follow a similar seasonal trend, reaching peak concentration

in summer. The summer high for NO_2 and SO_2 are 20 ppb and 4.5 ppb respectively. The lowest median concentration for NO_2 is observed in the spring and fall months (5 ppb) whereas for SO_2, concentrations are lowest during spring (2.75 ppb). Both NO_2 and SO_2 are among the main products of forest fires (Lazaridis et al., 2008) and peak concentrations observed during summer may be a result of smoke from wildfires originating outside of Minnesota, in the western U.S. and Canada (MPCA, 2019).

The concentration of O_3 (Figure 3.1(a)) peaks during summer season, reaching a maximum of approximately 38 ppb (summer 2021). The minimum concentration of O_3 observed is a winter low of 9 ppb (winter 2020). The higher levels of O_3 during the summer reflects increased photochemical activity during warmer months (US EPA, 2003).When compared to the rest of the pollutants, $PM_{2.5}$ (Figure 3.1(c)), PM_{10} (Figure 3.1(g)) and NO (Figure 3.1(f)) do not exhibit significant seasonal variations. However, it can be observed that both $PM_{2.5}$ and PM_{10} follow a similar trend and that median concentrations are highest during winter months (11.5 µg/m³ and 20 µg/m³ for $PM_{2.5}$ and PM_{10} respectively). NO experiences lower concentrations during the summer than in any of the other three seasons (1 ppb).

3.2. DIURNAL VARIABILITY

Figure 3.2, (a) through (g) illustrates daily trends for each of the pollutants in 2019 (blue), 2020 (purple) and 2021(green). Based on the plots generated, no significant variation is observed throughout the day for $PM_{2.5}$ (Figure 3.2(a)) (in the range of 4-6 µg/m³), PM_{10} (Figure 3.2(b)) (10-12 µg/m³) compared to the rest of the pollutants (CO, O_3, NO_2, NO, SO_2). The results for CO (Figure 3.2(c)) show that a peak concentration is

reached within 7.00 AM - 8.00 AM, which can be attributed to the morning rush (Jayaratne et al., 2021). After the morning rush hours, median CO concentration levels continue to decline to a minima of 290 ppb in the hours of early afternoon, between 2.00 PM -3.00 PM possibly due to lower traffic volumes or the contribution in photochemical reactions as a precursor compound for ozone formation. It can be observed that the CO concentration increases after 3.00 PM, possibly reflecting the evening rush hours (Jayaratne et al., 2021) and reaches another peak at about 10.00 PM.

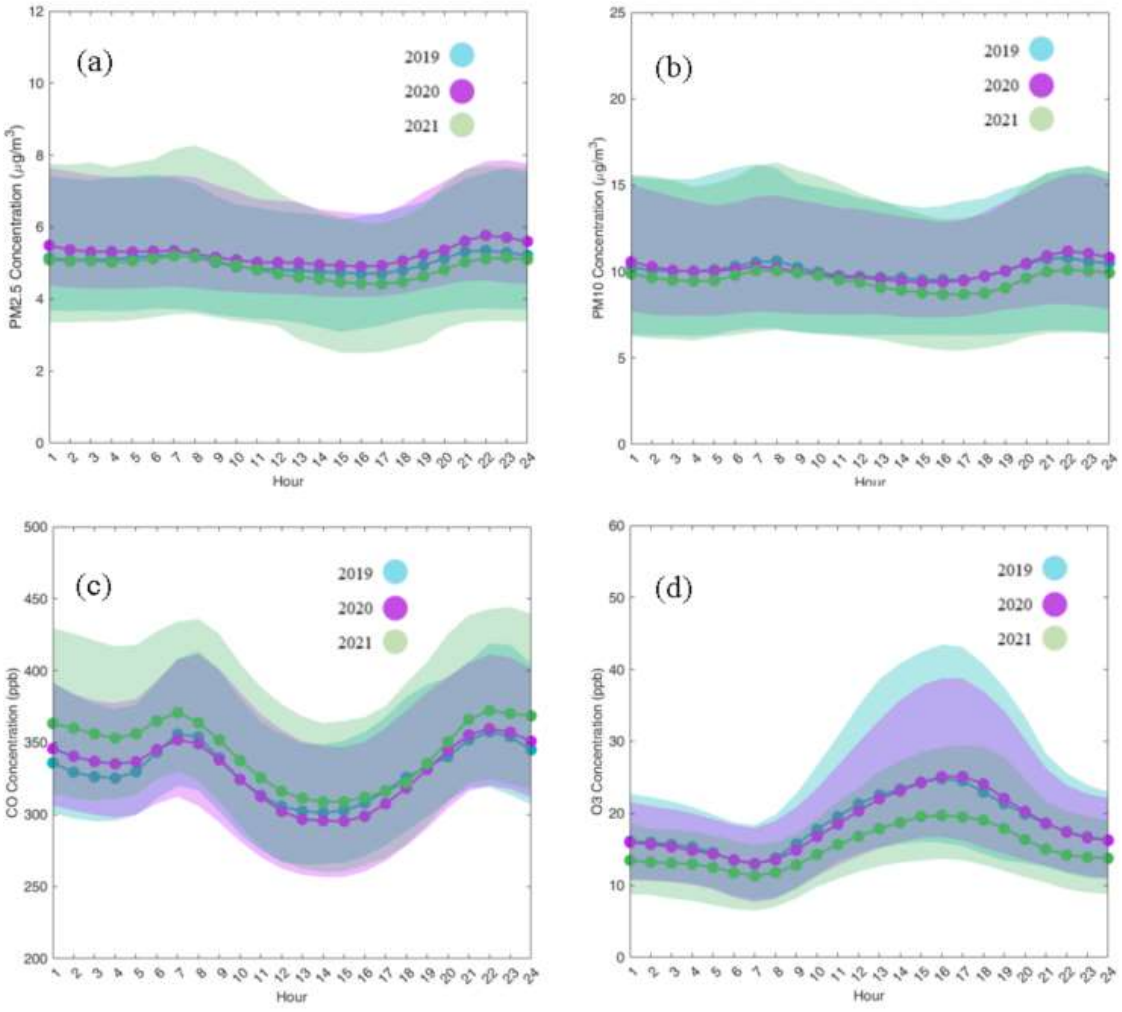

Figure 3.2 Daily trends of overall network

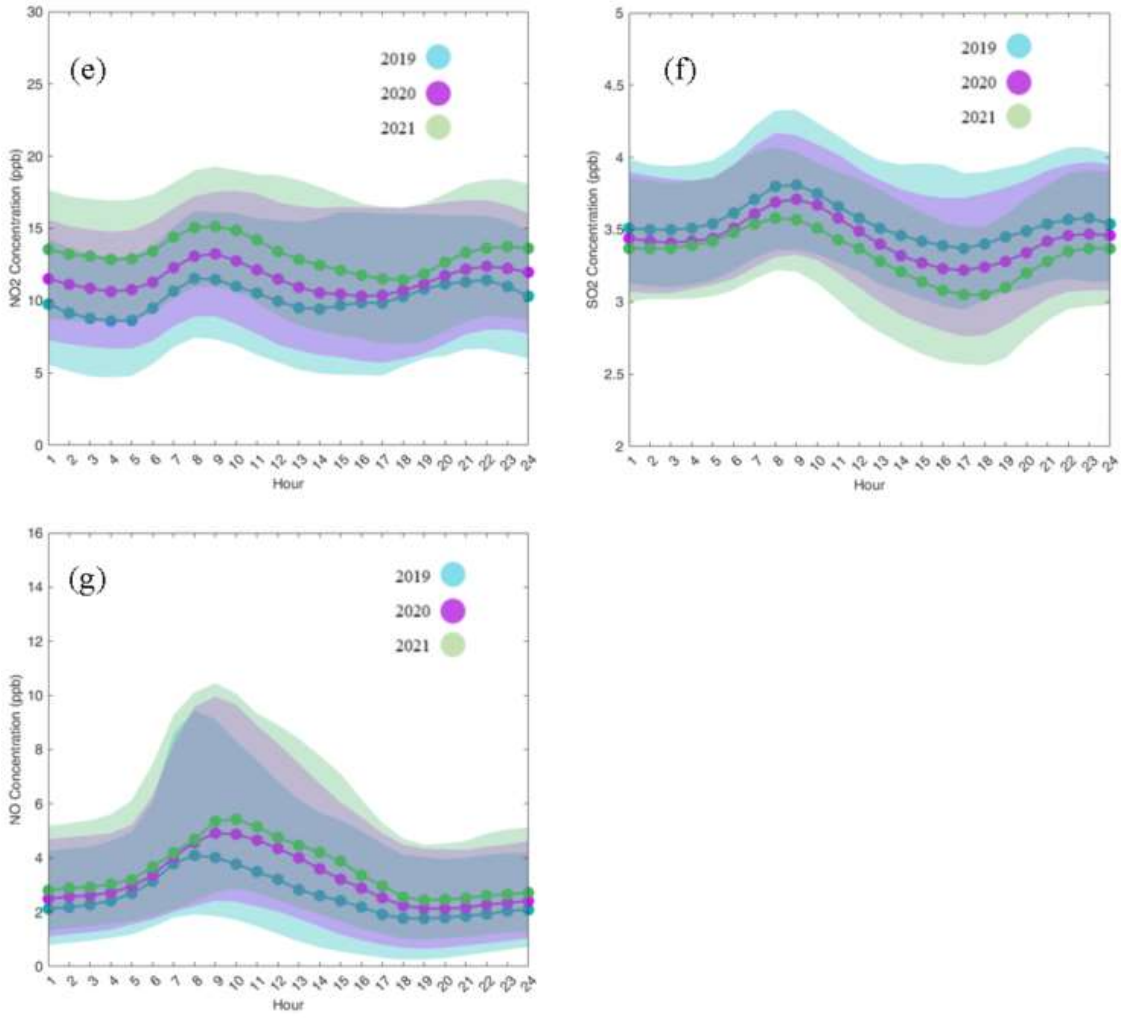

Figure 3.2 Daily trends of overall network. (Cont.)

O_3 concentration (Figure 3.2(d)) levels are observed to rise after 7.00 AM, in the presence of sunlight and peak concentrations are observed within the afternoon hours of 4.00 PM- 5.00 PM (24 ppb, 24 ppb and 19 ppb in 2019, 2020 and 2021 respectively). This peak in the late afternoon may be attributed to increased photochemical activity (Aneja et al., 2000). O_3 concentrations are found to decline as the intensity of sunlight reduces, after about 5.00 PM. NO (Figure 3.2(g)), NO_2 (Figure 3.2(e)) and SO_2 (Figure 3.2(f)), follow a

similar hourly trend, reaching a peak around 8.00 AM-9.00 AM, possibly due to the morning rush (Kendrick et al.,2015; Souza et al.,2019) .A minima is reached around 5.00 PM - 6.00 PM after which increasing concentrations are observed for NO_2 and SO_2, indicative of evening rush(Kendrick et al.,2015; Souza et al.,2019). However, for NO, a noticeable increase in concentration is not observed after the late afternoon minima. The highest median concentrations observed for NO, NO_2 and SO_2 are 5 ppb, 15 ppb and 3.75 ppb respectively.

It can be observed that for each pollutant, the results from years 2019-2021 all follow a similar general diurnal pattern thereby demonstrating the performance of the studied low-cost sensor network. It is also important to note that when compared to NAAQS, the concentrations observed are considerably lower.

3.3. SPATIAL VARIABILITY (COEFFICIENT OF DIVERGENCE)

Based on the results (see Appendix A), the maximum COD values computed are associated with concentrations of NO (Figure A.6) and are within the range of 0.2 - 0.65, indicating moderate to high spatial heterogeneity (Krudysz et al., 2008). All pairwise COD values for NO are greater than or equal to 0.2 and about half of the values are greater than 0.4. For NO_2 (Figure A.3), COD values range from 0.09 to 0.31 and about half of the site pairs show COD greater than 0.2. It can be observed that COD values of O_3 (Figure A.4) vary from 0.08 to 0.34 and those of PM_{10} (Figure A.7) are within the range of 0.09 -0.21. The range of COD values computed for NO_2, O_3 and PM_{10} indicate spatial homogeneity and modest spatial heterogeneity (Pakbin et al., 2010).The COD values calculated for concentrations of $PM_{2.5}$ (Figure A.1), CO (Figure A.2) and SO_2 (Figure A.5) vary between

0.06 - 0.13, 0.03- 0.17 and 0.03- 0.11 respectively, indicating little to no spatial variability (Pakbin et al., 2010).

3.4. SPECTRAL ANALYSIS

This section presents the results from power spectral analyses, identifying significant temporal cycles within the data separated into seasons. Results are summarized in Table 3.1 below. Based on the results obtained, daily, half month, monthly and month and a half cycles can be observed within the seasonal data. During the spring of 2020, daily cycles are dominant for all pollutants except for Particulate Matter ($PM_{2.5}$, PM_{10}). During the winter of 2019, monthly cycles are dominant for all pollutants except for NO, for which a daily periodicity is dominant.

Table 3.1 Key temporal cycles within pollutant concentration data.

	Dominant Periodicity (Days)							
Pollutant	SM19	FL19	WN19	SP20	SM20	FL20	WN20	SP21
$PM_{2.5}$	15	15	30	15	45	15	45	23
O_3	1	1	30	1	1	1	45	45
CO	1	45	30	1	1	1	45	1
NO_2	1	45	30	1	1	1	30	15
SO_2	45	45	30	1	45	13	45	1
NO	1	45	1	1	1	1	9	45
PM_{10}	15	10	30	15	45	15	45	23

3.5. EXPOSURE DISPARITIES BY INCOME

Figures 3.3(a) through (n) below illustrate the comparisons between median pollutant concentrations in the years 2019 vs. 2020 among the "high income" (Cedar-Isles-Dean, Highland Park Middle School, MPCA Office) and "low income" sites (Jackson Elementary School, Hawthorne, Bruce Vento Elementary School) selected (site selection introduced under materials and methods).By comparing the median CO concentrations in 2019 (Figure 3.3(a)) and 2020 (Figure 3.3(b)), it can be observed that the three low income sites (red) have higher concentrations in both 2019 (ranging from 300 - 400 ppb) and 2020 (300 - 410 ppb range) throughout most hours of the day relative to the concentrations of the three sites of higher income (blue) in 2019 (275-360 ppb range) and 2020 (260-360 ppb range).

Figure 3.3(c) and 3.3(d) illustrate the median pollutant concentrations of $PM_{2.5}$ in 2019 vs. 2020. While there is no apparent pollutant trend among high income and low income sites collectively, when examining the fluctuations in median $PM_{2.5}$ levels for the selected sites individually, it can be observed that there is a slight increase in concentration for two out of the three low income sites (namely, Hawthorne and Bruce Vento Elementary School) when comparing the years 2019 (5.1 ppb- 6 ppb for Hawthorne and 4.9 ppb- 6 ppb for BVES) and 2020 (5.4 ppb – 6.25 ppb for Hawthorne and 5.2 ppb -6.4 ppb for BVES). We also find that for two out of the three high income sites (namely, Cedar-Isles-Dean and Highland Park Middle School), a slight decrease in concentration is observed from 2019 (5.4 ppb – 6.3ppb range for CID and 5.7ppb- 6 ppb range for HPMS) to 2020 (5.3 ppb- 6.1 ppb range for CID and 5.3 ppb – 5.8ppb range for HPMS) at all hours.

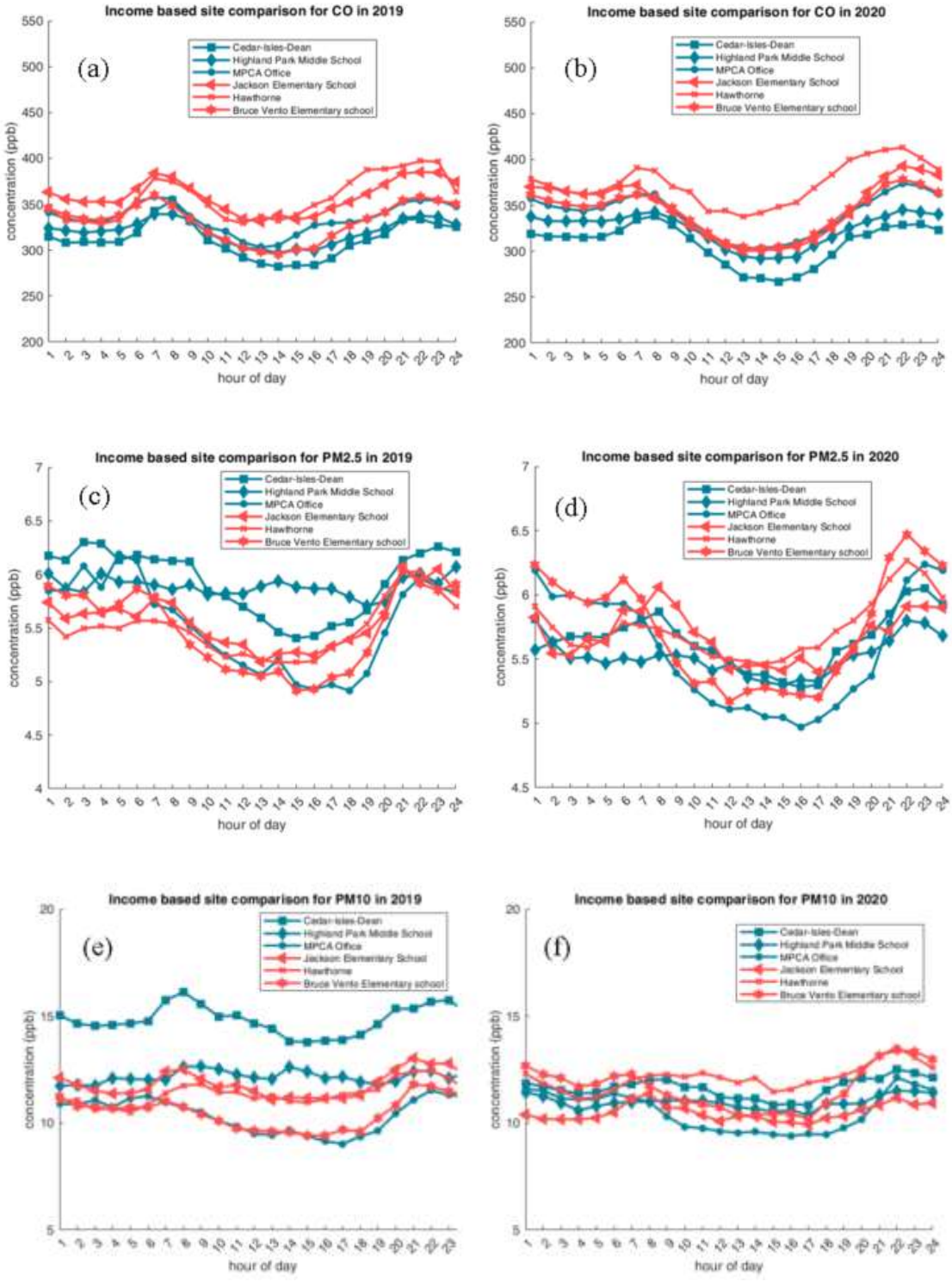

Figure 3.3 Income based site comparisons 2019 vs. 2020.

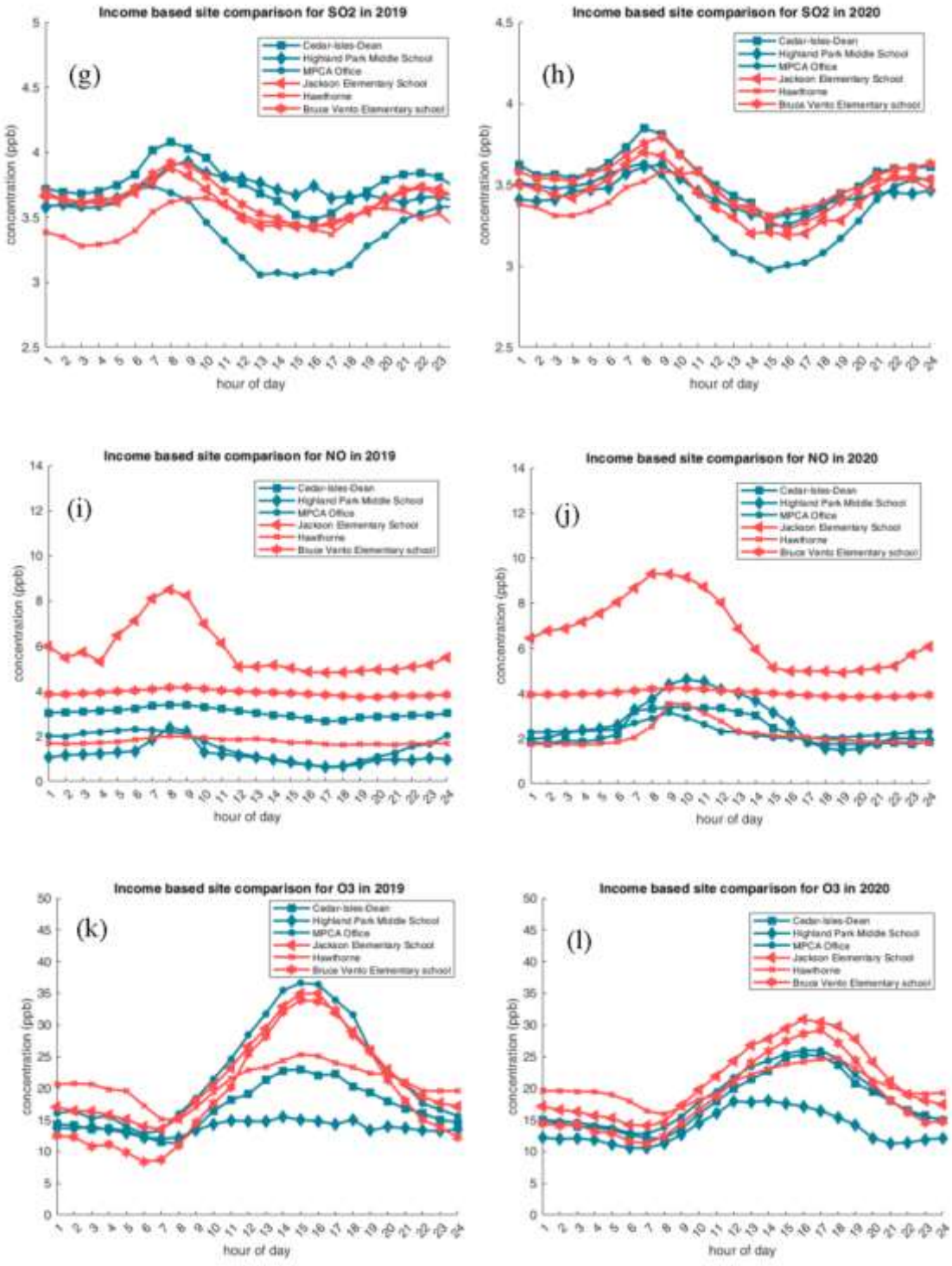

Figure 3.3 Income based site comparisons 2019 vs. 2020. (Cont.)

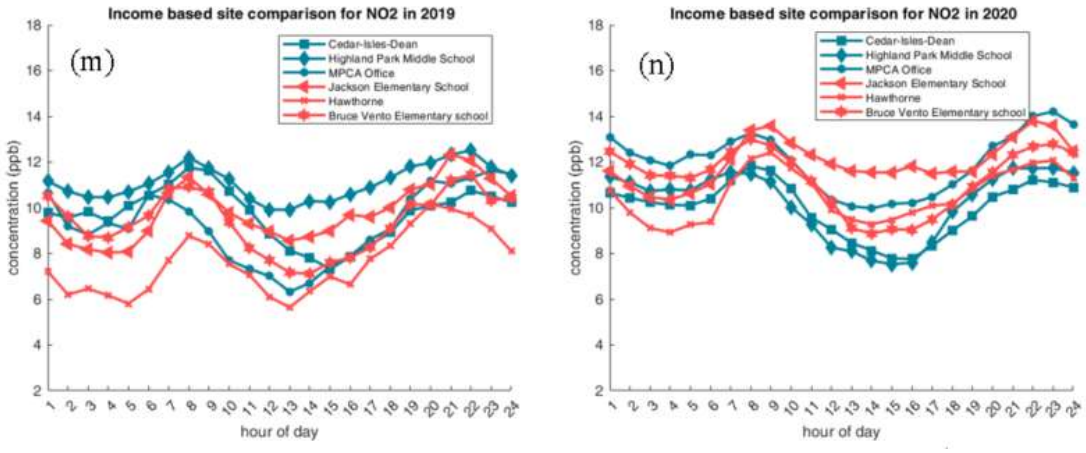

Figure 3.3 Income based site comparisons 2019 vs. 2020. (Cont.)

Table 3.2 below shows the correlation between per capita income and median pollutant concentrations. The correlation between median pollutant concentration over the years 2019 and 2021 and income is represented by "r_2019_2021" whereas "r_2019", "r_2020" and "r_2021" each represents the correlation between median pollutant concentration during that respective year and income. The correlation between percent reduction in median pollutant concentration over 2019-2021 and income is represented by "r_reduction".

Table 3.2 Correlation between median pollutant concentration and income.

Pollutant	**r_2019**	**r_2020**	**r_2021**	**r_2019_2021**	**r_reduction**
CO	-0.1365	0.0826	0.1987	0.1597	0.1541
NO	0.0959	-0.0369	0.0069	0.0154	0.0574
NO_2	0.2656	-0.0182	0.1711	0.3084	-0.1174

Table 3.2 Correlation between median pollutant concentration and income. (Cont.)

O_3	0.2264	-0.1548	0.1971	0.2092	-0.3059
PM_{10}	0.0564	0.0006	-0.0814	-0.043	-0.1063
PM_{25}	0.0094	-0.0268	-0.0436	-0.0983	-0.0469
SO_2	-0.3896	0.1592	0.0062	-0.0585	-0.2605

The Pearson correlation coefficients calculated indicate weak positive and weak negative correlations between per capita income and median pollutant concentrations over the years 2019-2021. Correlations between per capita income and median CO, NO, NO_2 and O_3 concentrations over 2019-2021 are weak positive (0.1597, 0.0154, 0.3084 and 0.2092 respectively) whereas PM_{10}, $PM_{2.5}$ and SO_2 show weak negative correlations (-0.043, -0.0983 and -0.0585 respectively). Per capita income and median NO_2 show the highest positive correlation of r =0.3084. Percent reduction in concentrations over 2019-2021 were found to be weakly negatively correlated with per capita income for all pollutants except for CO and NO which exhibited weak positive correlations (0.1541 and 0.0574 respectively).

The use of a SLR model suggested that there is no statistically significant linear relationship between per capita income and overall median pollutant concentrations except for NO_2. The SLR model fitted between NO_2 and per capita income had a p value=0.0417 < α=0.05 indicating a significant linear relationship between the two variables. High p-values (> α = 0.05) yielded from the Mann-Whitney U test, suggests that there is no

statistically significant difference between the pollutant levels of high income and low income sites.

3.6. EXPOSURE DISPARITIES BY HOLC GRADE

From the box-whisker plots of concentration vs. HOLC grade, it can be concluded that there is no significant variation in median concentration levels among site groups of HOLC grades, B, C and D. The median CO concentrations for groups B, C and D are within the range of 300-350 ppb. Median $PM_{2.5}$ varies within the range of 2-5 µg/m³ and median levels of PM_{10} range from 6-10 µg/m³. O_3, NO, NO_2, and SO_2 lie within the ranges of 15-17 ppb, 0.5-2 ppb, 10-12 ppb and 3.25-3.75 ppb respectively.

3.7. SOURCE CHARACTERIZATION (CBPF)

The CBPF results for gaseous pollutants, CO, O_3, NO_2, NO, SO_2 and particulate matter fractions, PM_{10}, $PM_{2.5}$ are included in the Appendix section of this paper. The plots generated (see Appendix B), illustrate seasonal variation over a one-year period (2020). It can be observed that similarities exist among dispersion of $PM_{2.5}$ and PM_{10}, notably in the spring and in the fall. In the spring (Figure B.1 and Figure B.25), highest probabilities for high concentrations appear in a southerly direction at relatively high wind speeds (between 8 m s^{-1} to 12 m s^{-1}). During the fall (Figure B.3 and Figure B.27), high probability areas occur under relatively low wind speed conditions (lower than 6 m s^{-1} for a majority of the sites) under which directionality is not well defined. Therefore, we can infer that, in the spring, sources that contribute to high concentrations of $PM_{2.5}$ and PM_{10} are not in the

immediate vicinity whereas dominant sources for high concentrations during fall are local in origin.

Figures B.13, B.14, B.15 and B.16 present the results for SO_2 in the spring (SP20), summer (SM20), fall (FL20) and winter (WN20), in that order. During SP20, FL20 and WN20, probability is highest under low wind speeds (<4 ms^{-1} for SP20, <2 m s^{-1} for FL20 and <4 m s^{-1} for WN20), indicating that local sources contribute to high concentrations. In SM20, areas of high probability appear toward a southwesterly direction at relatively high wind speeds (between 6 m s^{-1} and 10 ms^{-1}). Thus, it can be deduced that long range transport may contribute to high SO_2 concentrations during SM20. Interestingly, a peak in SO_2 concentration is observed during SM20 in the seasonal time variation plots (Figure 3.1(e)). The seasonal time variation plots also show that SO_2 and NO_2 (Figure 3.1(d)) follow a similar trend and a peak in NO_2 concentration is observed during SM20 as well. When comparing the CBPF plots of SO_2 and NO_2 during SM20, it can be seen that the dispersion pattern of NO_2 closely resembles to that of SO_2, indicating that NO_2 is transported. These results support the previous interpretation that the peak concentrations of SO_2 and NO_2 observed during SM20 may be owing to emissions from wildfires originating outside of Minnesota, in the Western United States and Canada.

4. CONCLUSION

A dense network of 45 low-cost multi-pollutant air quality sensors were deployed in Twin cities, Minnesota over the years 2019-2021 under MPCA's Assessing Urban Air Quality Project. Through the data analyses conducted, clear trends are observed for daily and monthly pollutant concentrations, which can be explained by traffic routines and atmospheric chemistry. Assessment of spatial variability between sensor sites indicates spatial homogeneity and modest spatial heterogeneity for all pollutants except NO, for which moderate to high spatial heterogeneity is observed. CBPF plots generated help identify impacts from local and distant emission sources and clear variation is observed across seasons. Also, the monthly pollution peaks observed for certain pollutants (SO_2, NO_2) can be justified through long range transportation, as indicated by the CBPF plots. Daily, semimonthly, monthly and month and a half cycles are dominant within the time series separated into seasons. Several statistical methods were used to evaluate exposure disparity across income groups in the city-scale and although some disparity is observed between sites of highest and lowest income, overall, it can be concluded that there is little to no correlation between pollutant exposure and income for the 45 locations studied in this work. There is no significant variation in median concentration levels among site groups of different redlining grades. However, replicating these analyses for low-cost sensor networks deployed elsewhere can deliver insight as to whether such exposure disparities exist within other urban areas.

APPENDIX A.

COEFFICIENTS OF DIVERGENCE (COD)

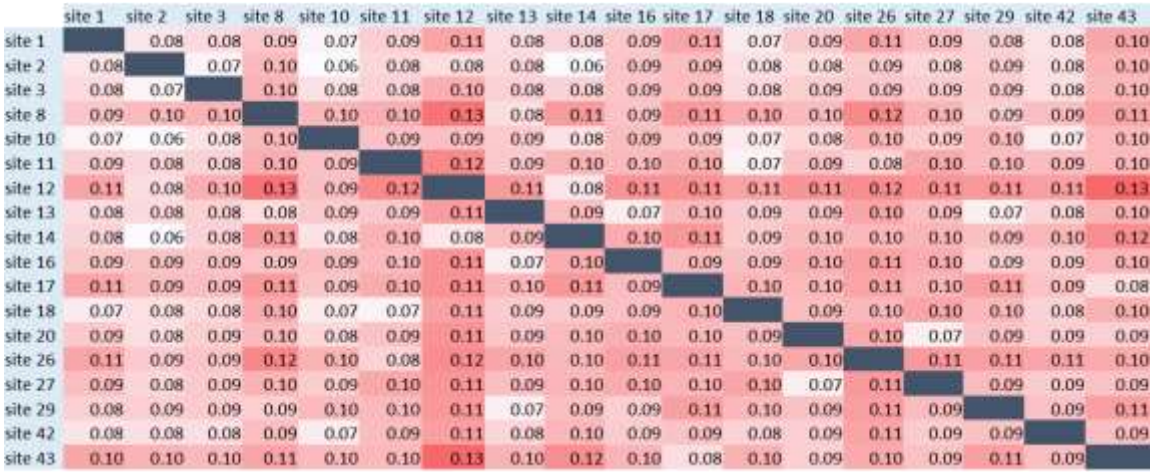

	site 1	site 2	site 3	site 8	site 10	site 11	site 12	site 13	site 14	site 16	site 17	site 18	site 20	site 26	site 27	site 29	site 42	site 43
site 1		0.08	0.08	0.09	0.07	0.09	0.11	0.08	0.08	0.09	0.11	0.07	0.09	0.11	0.09	0.08	0.08	0.10
site 2	0.08		0.07	0.10	0.06	0.08	0.08	0.08	0.06	0.09	0.09	0.08	0.08	0.09	0.08	0.09	0.08	0.10
site 3	0.08	0.07		0.10	0.08	0.08	0.10	0.08	0.08	0.09	0.09	0.08	0.09	0.09	0.09	0.09	0.08	0.10
site 8	0.09	0.10	0.10		0.10	0.10	0.13	0.08	0.11	0.09	0.11	0.10	0.10	0.12	0.10	0.09	0.09	0.11
site 10	0.07	0.06	0.08	0.10		0.09	0.09	0.09	0.08	0.09	0.09	0.07	0.08	0.10	0.09	0.10	0.07	0.10
site 11	0.09	0.08	0.08	0.10	0.09		0.12	0.09	0.10	0.10	0.10	0.07	0.09	0.08	0.10	0.10	0.09	0.10
site 12	0.11	0.08	0.10	0.13	0.09	0.12		0.11	0.08	0.11	0.11	0.11	0.11	0.12	0.11	0.11	0.11	0.13
site 13	0.08	0.08	0.08	0.08	0.09	0.09	0.11		0.09	0.07	0.10	0.09	0.09	0.10	0.09	0.07	0.08	0.10
site 14	0.08	0.06	0.08	0.11	0.08	0.10	0.08	0.09		0.10	0.11	0.09	0.10	0.10	0.10	0.09	0.10	0.12
site 16	0.09	0.09	0.09	0.09	0.09	0.10	0.11	0.07	0.10		0.09	0.09	0.10	0.11	0.10	0.09	0.09	0.10
site 17	0.11	0.09	0.09	0.11	0.09	0.10	0.11	0.10	0.11	0.09		0.10	0.10	0.11	0.10	0.11	0.09	0.08
site 18	0.07	0.08	0.08	0.10	0.07	0.07	0.11	0.09	0.09	0.09	0.10		0.09	0.10	0.10	0.10	0.08	0.10
site 20	0.09	0.08	0.09	0.10	0.08	0.09	0.11	0.09	0.10	0.10	0.10	0.09		0.10	0.07	0.09	0.09	0.09
site 26	0.11	0.09	0.09	0.12	0.10	0.08	0.12	0.10	0.10	0.11	0.11	0.10	0.10		0.11	0.11	0.11	0.10
site 27	0.09	0.08	0.09	0.10	0.09	0.10	0.11	0.09	0.10	0.10	0.10	0.10	0.07	0.11		0.09	0.09	0.09
site 29	0.08	0.09	0.09	0.09	0.10	0.10	0.11	0.07	0.09	0.09	0.11	0.10	0.09	0.11	0.09		0.09	0.11
site 42	0.08	0.08	0.08	0.09	0.07	0.09	0.11	0.08	0.10	0.09	0.09	0.08	0.09	0.11	0.09	0.09		0.09
site 43	0.10	0.10	0.10	0.11	0.10	0.10	0.13	0.10	0.12	0.10	0.08	0.10	0.09	0.10	0.09	0.11	0.09	

Figure A.1. COD for $PM_{2.5}$ (2020). COD> 0.2 significant difference

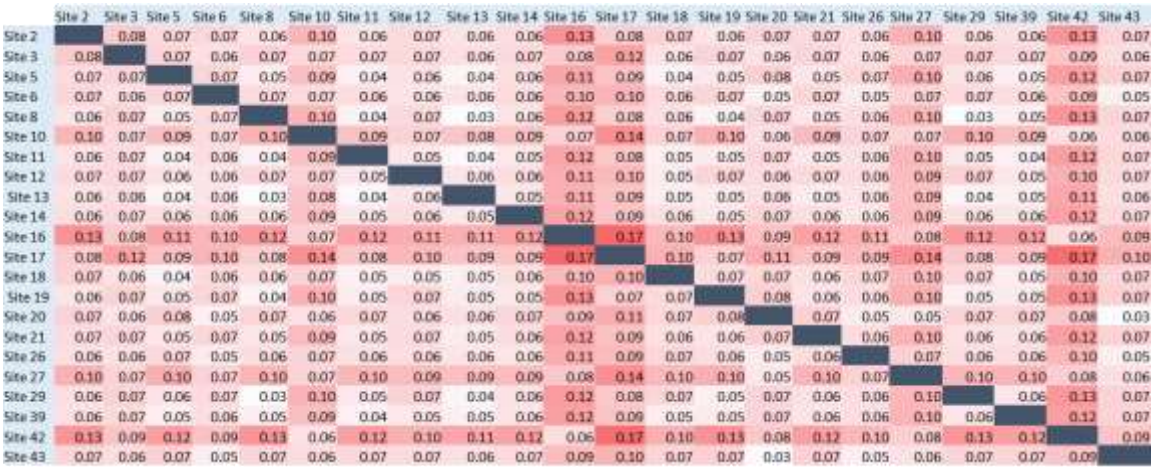

	Site 2	Site 3	Site 5	Site 6	Site 8	Site 10	Site 11	Site 12	Site 13	Site 14	Site 16	Site 17	Site 18	Site 19	Site 20	Site 21	Site 26	Site 27	Site 29	Site 39	Site 42	Site 43
Site 2		0.08	0.07	0.07	0.06	0.10	0.06	0.07	0.06	0.06	0.13	0.08	0.07	0.06	0.07	0.07	0.06	0.10	0.06	0.06	0.13	0.07
Site 3	0.08		0.07	0.06	0.07	0.07	0.07	0.07	0.06	0.07	0.08	0.12	0.06	0.07	0.06	0.07	0.06	0.07	0.07	0.07	0.09	0.06
Site 5	0.07	0.07		0.07	0.05	0.09	0.04	0.06	0.04	0.06	0.11	0.09	0.04	0.05	0.08	0.05	0.07	0.10	0.06	0.05	0.12	0.07
Site 6	0.07	0.06	0.07		0.07	0.07	0.06	0.06	0.06	0.06	0.10	0.10	0.06	0.07	0.05	0.07	0.05	0.07	0.07	0.06	0.09	0.05
Site 8	0.06	0.07	0.05	0.07		0.10	0.04	0.07	0.03	0.06	0.12	0.08	0.06	0.04	0.07	0.05	0.06	0.10	0.03	0.05	0.13	0.07
Site 10	0.10	0.07	0.09	0.07	0.10		0.09	0.07	0.08	0.09	0.07	0.14	0.07	0.10	0.06	0.09	0.07	0.07	0.10	0.09	0.06	0.06
Site 11	0.06	0.07	0.04	0.06	0.04	0.09		0.05	0.04	0.05	0.12	0.08	0.05	0.05	0.07	0.05	0.06	0.10	0.05	0.04	0.12	0.07
Site 12	0.07	0.07	0.06	0.06	0.07	0.07	0.05		0.06	0.06	0.11	0.10	0.05	0.07	0.06	0.07	0.06	0.09	0.07	0.05	0.10	0.07
Site 13	0.06	0.06	0.04	0.06	0.03	0.08	0.04	0.06		0.05	0.11	0.09	0.05	0.05	0.06	0.05	0.06	0.09	0.04	0.05	0.11	0.06
Site 14	0.06	0.07	0.06	0.06	0.06	0.09	0.05	0.06	0.05		0.12	0.09	0.06	0.05	0.07	0.06	0.06	0.09	0.06	0.06	0.12	0.07
Site 16	0.13	0.08	0.11	0.10	0.12	0.07	0.12	0.11	0.11	0.12		0.17	0.10	0.13	0.09	0.12	0.11	0.08	0.12	0.12	0.06	0.09
Site 17	0.08	0.12	0.09	0.10	0.08	0.14	0.08	0.10	0.09	0.09	0.17		0.10	0.07	0.11	0.09	0.09	0.14	0.08	0.09	0.17	0.10
Site 18	0.07	0.06	0.04	0.06	0.06	0.07	0.05	0.05	0.05	0.06	0.10	0.10		0.07	0.07	0.06	0.07	0.10	0.07	0.05	0.10	0.07
Site 19	0.06	0.07	0.05	0.07	0.04	0.10	0.05	0.07	0.05	0.05	0.13	0.07	0.07		0.08	0.06	0.06	0.10	0.05	0.05	0.13	0.07
Site 20	0.07	0.06	0.08	0.05	0.07	0.06	0.07	0.06	0.06	0.07	0.09	0.11	0.07	0.06		0.07	0.05	0.05	0.07	0.07	0.08	0.03
Site 21	0.07	0.07	0.05	0.07	0.05	0.09	0.05	0.07	0.05	0.06	0.12	0.09	0.06	0.06	0.07		0.06	0.10	0.06	0.06	0.12	0.07
Site 26	0.06	0.06	0.07	0.05	0.06	0.07	0.06	0.06	0.06	0.06	0.11	0.09	0.07	0.06	0.05	0.06		0.07	0.06	0.06	0.10	0.05
Site 27	0.10	0.07	0.10	0.07	0.10	0.07	0.10	0.09	0.09	0.09	0.08	0.14	0.10	0.10	0.05	0.10	0.07		0.10	0.10	0.08	0.06
Site 29	0.06	0.07	0.06	0.07	0.03	0.10	0.05	0.07	0.04	0.06	0.12	0.08	0.07	0.05	0.07	0.06	0.06	0.10		0.06	0.13	0.07
Site 39	0.06	0.07	0.05	0.06	0.05	0.09	0.04	0.05	0.05	0.06	0.12	0.09	0.05	0.05	0.07	0.06	0.06	0.10	0.06		0.12	0.07
Site 42	0.13	0.09	0.12	0.09	0.13	0.06	0.12	0.10	0.11	0.12	0.06	0.17	0.10	0.13	0.08	0.12	0.10	0.08	0.13	0.12		0.09
Site 43	0.07	0.06	0.07	0.05	0.07	0.06	0.07	0.07	0.06	0.07	0.09	0.10	0.07	0.07	0.03	0.07	0.05	0.06	0.07	0.07	0.09	

Figure A.2. COD for CO (2020). COD> 0.2 significant difference

	Site 2	Site 3	Site 5	Site 6	Site 8	Site 10	Site 11	Site 12	Site 13	Site 14	Site 16	Site 17	Site 18	Site 19	Site 20	Site 21	Site 26	Site 27	Site 29	Site 39	Site 42	Site 43
Site 2		0.22	0.17	0.19	0.21	0.20	0.21	0.20	0.19	0.25	0.18	0.17	0.24	0.18	0.22	0.25	0.23	0.21	0.21	0.21	0.22	0.21
Site 3	0.22		0.22	0.20	0.18	0.15	0.20	0.14	0.18	0.18	0.18	0.19	0.15	0.20	0.21	0.30	0.13	0.17	0.19	0.23	0.20	0.21
Site 5	0.17	0.22		0.17	0.21	0.19	0.17	0.19	0.17	0.24	0.20	0.19	0.22	0.14	0.24	0.22	0.24	0.22	0.19	0.17	0.21	0.19
Site 6	0.19	0.20	0.17		0.20	0.14	0.20	0.17	0.18	0.18	0.21	0.18	0.17	0.18	0.24	0.22	0.23	0.22	0.20	0.20	0.24	0.23
Site 8	0.21	0.18	0.21	0.20		0.19	0.21	0.18	0.13	0.22	0.16	0.18	0.21	0.21	0.24	0.28	0.20	0.18	0.16	0.24	0.21	0.23
Site 10	0.20	0.15	0.19	0.14	0.19		0.22	0.14	0.19	0.14	0.19	0.17	0.12	0.21	0.20	0.26	0.18	0.19	0.21	0.23	0.23	0.23
Site 11	0.21	0.20	0.17	0.20	0.21	0.22		0.18	0.15	0.25	0.23	0.21	0.25	0.09	0.23	0.26	0.20	0.19	0.14	0.09	0.12	0.11
Site 12	0.20	0.14	0.19	0.17	0.18	0.14	0.18		0.16	0.18	0.19	0.16	0.17	0.17	0.21	0.27	0.16	0.17	0.17	0.20	0.19	0.19
Site 13	0.19	0.18	0.17	0.18	0.13	0.19	0.15	0.16		0.23	0.17	0.17	0.22	0.16	0.23	0.25	0.20	0.17	0.12	0.18	0.17	0.18
Site 14	0.25	0.18	0.24	0.18	0.22	0.14	0.25	0.18	0.23		0.23	0.21	0.13	0.24	0.26	0.30	0.20	0.22	0.24	0.27	0.27	0.26
Site 16	0.18	0.18	0.20	0.21	0.16	0.19	0.23	0.19	0.17	0.23		0.18	0.21	0.22	0.23	0.28	0.21	0.20	0.20	0.25	0.23	0.24
Site 17	0.17	0.19	0.19	0.18	0.18	0.17	0.21	0.16	0.17	0.21	0.18		0.21	0.19	0.23	0.26	0.19	0.15	0.18	0.23	0.22	0.20
Site 18	0.24	0.15	0.22	0.17	0.21	0.12	0.25	0.17	0.22	0.13	0.21	0.21		0.24	0.24	0.29	0.20	0.22	0.24	0.26	0.26	0.26
Site 19	0.18	0.20	0.14	0.18	0.21	0.21	0.09	0.17	0.16	0.24	0.22	0.19	0.24		0.24	0.24	0.21	0.19	0.16	0.10	0.14	0.11
Site 20	0.22	0.21	0.24	0.24	0.24	0.20	0.23	0.21	0.23	0.26	0.23	0.23	0.24	0.24		0.31	0.21	0.22	0.23	0.24	0.22	0.22
Site 21	0.25	0.30	0.22	0.22	0.28	0.26	0.26	0.27	0.25	0.30	0.28	0.26	0.29	0.24	0.31		0.31	0.29	0.26	0.26	0.30	0.28
Site 26	0.23	0.13	0.24	0.23	0.20	0.18	0.20	0.16	0.20	0.20	0.21	0.19	0.20	0.21	0.21	0.31		0.16	0.18	0.23	0.19	0.20
Site 27	0.21	0.17	0.22	0.22	0.18	0.19	0.19	0.17	0.17	0.22	0.20	0.15	0.22	0.19	0.22	0.29	0.16		0.17	0.21	0.18	0.17
Site 29	0.21	0.19	0.19	0.20	0.16	0.21	0.14	0.17	0.12	0.24	0.20	0.18	0.24	0.16	0.23	0.26	0.18	0.17		0.17	0.16	0.16
Site 39	0.21	0.23	0.17	0.20	0.24	0.23	0.09	0.20	0.18	0.27	0.25	0.23	0.26	0.10	0.24	0.26	0.23	0.21	0.17		0.15	0.12
Site 42	0.22	0.20	0.21	0.24	0.21	0.23	0.12	0.19	0.17	0.27	0.23	0.22	0.26	0.14	0.22	0.30	0.19	0.18	0.16	0.15		0.12
Site 43	0.21	0.21	0.19	0.23	0.23	0.23	0.11	0.19	0.18	0.26	0.24	0.20	0.26	0.11	0.22	0.28	0.20	0.17	0.16	0.12	0.12	

Figure A.3. COD for NO_2 (2020). COD> 0.2 significant difference

	Site 2	Site 3	Site 5	Site 6	Site 8	Site 10	Site 11	Site 12	Site 13	Site 14	Site 16	Site 17	Site 18	Site 19	Site 20	Site 21	Site 26	Site 27	Site 29	Site 39	Site 42	Site 43
Site 2		0.28	0.24	0.22	0.27	0.25	0.11	0.23	0.25	0.22	0.14	0.18	0.29	0.21	0.25	0.22	0.29	0.26	0.25	0.15	0.25	0.24
Site 3	0.28		0.15	0.16	0.18	0.12	0.30	0.15	0.13	0.13	0.25	0.22	0.25	0.16	0.19	0.26	0.14	0.13	0.17	0.32	0.16	0.16
Site 5	0.24	0.15		0.13	0.16	0.15	0.26	0.15	0.11	0.13	0.20	0.19	0.27	0.13	0.19	0.22	0.19	0.16	0.15	0.29	0.14	0.16
Site 6	0.22	0.16	0.13		0.19	0.12	0.24	0.09	0.12	0.08	0.18	0.15	0.26	0.10	0.17	0.18	0.18	0.13	0.15	0.26	0.16	0.12
Site 8	0.27	0.18	0.16	0.19		0.19	0.29	0.19	0.14	0.18	0.23	0.22	0.27	0.18	0.22	0.26	0.21	0.19	0.16	0.31	0.17	0.20
Site 10	0.25	0.12	0.15	0.12	0.19		0.27	0.11	0.12	0.10	0.23	0.17	0.26	0.13	0.15	0.23	0.14	0.11	0.16	0.30	0.14	0.12
Site 11	0.11	0.30	0.26	0.24	0.29	0.27		0.25	0.27	0.24	0.14	0.21	0.30	0.23	0.27	0.22	0.30	0.28	0.27	0.14	0.27	0.25
Site 12	0.23	0.15	0.15	0.09	0.19	0.11	0.25		0.13	0.09	0.20	0.17	0.24	0.13	0.18	0.21	0.18	0.14	0.16	0.27	0.17	0.14
Site 13	0.25	0.13	0.11	0.12	0.14	0.12	0.27	0.13		0.11	0.21	0.19	0.26	0.13	0.17	0.23	0.17	0.13	0.12	0.30	0.13	0.14
Site 14	0.22	0.13	0.13	0.08	0.18	0.10	0.24	0.09	0.11		0.19	0.16	0.24	0.11	0.16	0.20	0.15	0.12	0.14	0.27	0.15	0.12
Site 16	0.14	0.25	0.20	0.18	0.23	0.23	0.14	0.20	0.21	0.19		0.17	0.29	0.18	0.24	0.18	0.26	0.23	0.21	0.16	0.23	0.21
Site 17	0.18	0.22	0.19	0.15	0.22	0.17	0.21	0.17	0.19	0.16	0.17		0.29	0.14	0.20	0.21	0.22	0.18	0.19	0.23	0.18	0.14
Site 18	0.29	0.25	0.27	0.26	0.27	0.26	0.30	0.24	0.26	0.24	0.29	0.29		0.27	0.30	0.33	0.28	0.26	0.29	0.34	0.28	0.28
Site 19	0.21	0.16	0.13	0.10	0.18	0.13	0.23	0.13	0.13	0.11	0.18	0.14	0.27		0.18	0.18	0.18	0.15	0.15	0.26	0.15	0.12
Site 20	0.25	0.19	0.19	0.17	0.22	0.15	0.27	0.18	0.17	0.16	0.24	0.20	0.30	0.18		0.25	0.19	0.16	0.18	0.30	0.17	0.16
Site 21	0.22	0.26	0.22	0.18	0.26	0.23	0.22	0.21	0.23	0.20	0.18	0.21	0.33	0.18	0.25		0.27	0.24	0.23	0.24	0.25	0.21
Site 26	0.29	0.14	0.19	0.18	0.21	0.14	0.30	0.18	0.17	0.15	0.26	0.22	0.28	0.18	0.19	0.27		0.14	0.18	0.33	0.17	0.16
Site 27	0.26	0.13	0.16	0.13	0.19	0.11	0.28	0.14	0.13	0.12	0.23	0.18	0.26	0.15	0.16	0.24	0.14		0.15	0.30	0.14	0.10
Site 29	0.25	0.17	0.15	0.15	0.16	0.16	0.27	0.16	0.12	0.14	0.21	0.19	0.29	0.15	0.18	0.23	0.18	0.15		0.29	0.16	0.16
Site 39	0.15	0.32	0.29	0.26	0.31	0.30	0.14	0.27	0.30	0.27	0.16	0.23	0.34	0.26	0.30	0.24	0.33	0.30	0.29		0.30	0.28
Site 42	0.25	0.16	0.14	0.16	0.17	0.14	0.27	0.17	0.13	0.15	0.23	0.18	0.28	0.15	0.17	0.25	0.17	0.14	0.16	0.30		0.15
Site 43	0.24	0.16	0.16	0.12	0.20	0.12	0.25	0.14	0.14	0.12	0.21	0.14	0.28	0.12	0.16	0.21	0.16	0.10	0.16	0.28	0.15	

Figure A.4. COD for O_3 (2020). COD> 0.2 significant difference

	Site 2	Site 5	Site 6	Site 8	Site 10	Site 11	Site 13	Site 14	Site 16	Site 17	Site 18	Site 19	Site 20	Site 27	Site 29	Site 39	Site 42	Site 43
Site 2		0.08	0.08	0.08	0.09	0.08	0.07	0.09	0.06	0.05	0.08	0.08	0.07	0.07	0.11	0.07	0.07	0.08
Site 5	0.08		0.06	0.04	0.06	0.05	0.05	0.07	0.04	0.07	0.07	0.05	0.06	0.06	0.08	0.05	0.06	0.09
Site 6	0.08	0.06		0.06	0.05	0.06	0.06	0.06	0.07	0.06	0.07	0.06	0.06	0.05	0.07	0.05	0.05	0.09
Site 8	0.08	0.04	0.06		0.05	0.06	0.03	0.05	0.04	0.06	0.06	0.04	0.06	0.05	0.06	0.05	0.05	0.10
Site 10	0.09	0.06	0.05	0.05		0.06	0.05	0.04	0.06	0.07	0.06	0.04	0.06	0.06	0.07	0.05	0.07	0.11
Site 11	0.08	0.05	0.06	0.06	0.06		0.06	0.07	0.06	0.07	0.07	0.06	0.06	0.07	0.08	0.05	0.06	0.10
Site 13	0.07	0.05	0.06	0.03	0.05	0.06		0.06	0.04	0.06	0.07	0.05	0.06	0.06	0.08	0.05	0.06	0.10
Site 14	0.09	0.07	0.06	0.05	0.04	0.07	0.06		0.06	0.07	0.05	0.05	0.07	0.06	0.06	0.05	0.07	0.11
Site 16	0.06	0.04	0.07	0.04	0.06	0.06	0.04	0.06		0.06	0.06	0.06	0.06	0.06	0.09	0.05	0.06	0.10
Site 17	0.05	0.07	0.06	0.06	0.07	0.07	0.06	0.07	0.06		0.07	0.07	0.06	0.05	0.09	0.06	0.05	0.09
Site 18	0.08	0.07	0.07	0.06	0.06	0.07	0.07	0.05	0.06	0.07		0.06	0.08	0.07	0.08	0.05	0.07	0.10
Site 19	0.08	0.05	0.06	0.04	0.04	0.06	0.05	0.05	0.06	0.07	0.06		0.07	0.06	0.06	0.05	0.06	0.09
Site 20	0.07	0.06	0.06	0.06	0.06	0.06	0.06	0.07	0.06	0.06	0.08	0.07		0.06	0.09	0.06	0.06	0.10
Site 27	0.07	0.06	0.05	0.05	0.06	0.07	0.06	0.06	0.06	0.05	0.07	0.06	0.06		0.08	0.05	0.05	0.10
Site 29	0.11	0.08	0.07	0.06	0.07	0.08	0.08	0.06	0.09	0.09	0.08	0.06	0.09	0.08		0.08	0.08	0.11
Site 39	0.07	0.05	0.05	0.05	0.05	0.05	0.05	0.05	0.05	0.06	0.05	0.05	0.06	0.05	0.08		0.06	0.09
Site 42	0.07	0.06	0.05	0.05	0.07	0.06	0.06	0.07	0.06	0.05	0.07	0.06	0.06	0.05	0.08	0.06		0.09
Site 43	0.08	0.09	0.09	0.10	0.11	0.10	0.10	0.11	0.10	0.09	0.10	0.09	0.10	0.10	0.11	0.09	0.09	

Figure A.5. COD for SO_2 (2020). COD> 0.2 significant difference

	Site 2	Site 3	Site 5	Site 6	Site 8	Site 10	Site 11	Site 12	Site 13	Site 14	Site 16	Site 17	Site 18	Site 19	Site 20	Site 21	Site 26	Site 27	Site 29	Site 39	Site 42	Site 43
Site 2		0.45	0.42	0.57	0.41	0.37	0.34	0.44	0.33	0.39	0.34	0.39	0.38	0.58	0.46	0.30	0.50	0.51	0.43	0.42	0.37	0.58
Site 3	0.45		0.39	0.48	0.28	0.41	0.45	0.43	0.41	0.46	0.42	0.42	0.38	0.46	0.36	0.39	0.42	0.39	0.39	0.38	0.33	0.51
Site 5	0.42	0.39		0.60	0.31	0.30	0.38	0.47	0.36	0.50	0.41	0.47	0.32	0.58	0.44	0.38	0.48	0.51	0.36	0.45	0.30	0.63
Site 6	0.57	0.48	0.60		0.48	0.62	0.58	0.36	0.58	0.50	0.49	0.53	0.50	0.22	0.34	0.50	0.37	0.24	0.48	0.34	0.50	0.20
Site 8	0.41	0.28	0.31	0.48		0.35	0.41	0.39	0.37	0.42	0.35	0.40	0.31	0.47	0.35	0.33	0.43	0.39	0.38	0.35	0.31	0.51
Site 10	0.37	0.41	0.30	0.62	0.35		0.33	0.49	0.32	0.48	0.42	0.40	0.34	0.62	0.47	0.37	0.50	0.53	0.40	0.47	0.31	0.65
Site 11	0.34	0.45	0.38	0.58	0.41	0.33		0.46	0.36	0.48	0.42	0.40	0.34	0.59	0.45	0.37	0.47	0.51	0.40	0.44	0.33	0.61
Site 12	0.44	0.43	0.47	0.36	0.39	0.49	0.46		0.47	0.46	0.41	0.45	0.34	0.39	0.36	0.37	0.37	0.34	0.44	0.27	0.40	0.39
Site 13	0.33	0.41	0.36	0.58	0.37	0.32	0.36	0.47		0.43	0.35	0.39	0.38	0.59	0.45	0.34	0.50	0.51	0.36	0.42	0.31	0.61
Site 14	0.39	0.46	0.50	0.50	0.42	0.48	0.48	0.46	0.43		0.36	0.41	0.46	0.54	0.46	0.37	0.51	0.48	0.48	0.41	0.45	0.50
Site 16	0.34	0.42	0.41	0.49	0.35	0.42	0.42	0.41	0.35	0.36		0.43	0.39	0.52	0.43	0.29	0.49	0.46	0.43	0.36	0.38	0.51
Site 17	0.39	0.42	0.47	0.53	0.40	0.40	0.40	0.45	0.39	0.41	0.43		0.41	0.55	0.43	0.38	0.48	0.47	0.44	0.42	0.38	0.55
Site 18	0.38	0.38	0.32	0.50	0.31	0.34	0.34	0.34	0.38	0.46	0.39	0.41		0.50	0.38	0.32	0.40	0.41	0.39	0.34	0.31	0.53
Site 19	0.58	0.46	0.58	0.22	0.47	0.62	0.59	0.39	0.59	0.54	0.52	0.55	0.50		0.35	0.52	0.35	0.24	0.49	0.37	0.49	0.24
Site 20	0.46	0.36	0.44	0.34	0.35	0.47	0.45	0.36	0.45	0.46	0.43	0.43	0.38	0.35		0.41	0.32	0.21	0.33	0.30	0.33	0.38
Site 21	0.30	0.39	0.38	0.50	0.33	0.37	0.37	0.37	0.34	0.37	0.29	0.38	0.32	0.52	0.41		0.46	0.45	0.41	0.35	0.35	0.52
Site 26	0.50	0.42	0.48	0.37	0.43	0.50	0.47	0.37	0.50	0.51	0.49	0.48	0.40	0.35	0.32	0.46		0.29	0.39	0.35	0.39	0.41
Site 27	0.51	0.39	0.51	0.24	0.39	0.53	0.51	0.34	0.51	0.48	0.46	0.47	0.41	0.24	0.21	0.45	0.29		0.39	0.29	0.40	0.28
Site 29	0.43	0.39	0.36	0.48	0.38	0.40	0.40	0.44	0.36	0.48	0.43	0.44	0.39	0.49	0.33	0.41	0.39	0.39		0.38	0.29	0.53
Site 39	0.42	0.38	0.45	0.34	0.35	0.47	0.44	0.27	0.42	0.41	0.36	0.42	0.34	0.37	0.30	0.35	0.35	0.29	0.38		0.35	0.37
Site 42	0.37	0.33	0.30	0.50	0.31	0.31	0.33	0.40	0.31	0.45	0.38	0.38	0.31	0.49	0.33	0.35	0.39	0.40	0.29	0.35		0.54
Site 43	0.58	0.51	0.63	0.20	0.51	0.65	0.61	0.39	0.61	0.50	0.51	0.55	0.53	0.24	0.38	0.52	0.41	0.28	0.53	0.37	0.54	

Figure A.6. COD for NO (2020). COD> 0.2 significant difference

	site 1	site 2	site 3	site 8	site 10	site 11	site 12	site 13	site 14	site 16	site 17	site 18	site 20	site 26	site 27	site 29	site 42	site 43
site 1		0.11	0.09	0.12	0.09	0.10	0.16	0.09	0.12	0.11	0.15	0.10	0.10	0.12	0.11	0.10	0.11	0.14
site 2	0.11		0.10	0.16	0.12	0.12	0.13	0.11	0.09	0.15	0.18	0.13	0.11	0.12	0.13	0.11	0.13	0.18
site 3	0.09	0.10		0.14	0.09	0.10	0.15	0.10	0.12	0.12	0.14	0.10	0.10	0.12	0.10	0.11	0.11	0.13
site 8	0.12	0.16	0.14		0.13	0.14	0.21	0.12	0.17	0.13	0.16	0.14	0.13	0.16	0.13	0.13	0.13	0.14
site 10	0.09	0.12	0.09	0.13		0.11	0.15	0.11	0.13	0.11	0.12	0.10	0.11	0.13	0.10	0.12	0.10	0.12
site 11	0.10	0.12	0.10	0.14	0.11		0.17	0.11	0.13	0.13	0.15	0.09	0.11	0.12	0.12	0.11	0.12	0.14
site 12	0.16	0.13	0.15	0.21	0.15	0.17		0.16	0.12	0.17	0.19	0.17	0.16	0.17	0.17	0.16	0.17	0.21
site 13	0.09	0.11	0.10	0.12	0.11	0.11	0.16		0.12	0.10	0.15	0.12	0.11	0.13	0.11	0.09	0.11	0.15
site 14	0.12	0.09	0.12	0.17	0.13	0.13	0.12	0.12		0.16	0.19	0.14	0.12	0.12	0.14	0.12	0.15	0.19
site 16	0.11	0.15	0.12	0.13	0.11	0.13	0.17	0.10	0.16		0.13	0.12	0.14	0.16	0.12	0.12	0.12	0.13
site 17	0.15	0.18	0.14	0.16	0.12	0.15	0.19	0.15	0.19	0.13		0.14	0.16	0.17	0.13	0.16	0.13	0.11
site 18	0.10	0.13	0.10	0.14	0.10	0.09	0.17	0.12	0.14	0.12	0.14		0.12	0.14	0.12	0.13	0.11	0.13
site 20	0.10	0.11	0.10	0.13	0.11	0.11	0.16	0.11	0.12	0.14	0.16	0.12		0.12	0.09	0.11	0.12	0.14
site 26	0.12	0.12	0.12	0.16	0.13	0.12	0.17	0.13	0.12	0.16	0.17	0.14	0.12		0.13	0.13	0.14	0.16
site 27	0.11	0.13	0.10	0.13	0.10	0.12	0.17	0.11	0.14	0.12	0.13	0.12	0.09	0.13		0.12	0.11	0.11
site 29	0.10	0.11	0.11	0.13	0.12	0.11	0.16	0.09	0.12	0.12	0.16	0.13	0.11	0.13	0.12		0.12	0.16
site 42	0.11	0.13	0.11	0.13	0.10	0.12	0.17	0.11	0.15	0.12	0.13	0.11	0.12	0.14	0.11	0.12		0.13
site 43	0.14	0.18	0.13	0.14	0.12	0.14	0.21	0.15	0.19	0.13	0.11	0.13	0.14	0.16	0.11	0.16	0.13	

Figure A.7. COD for PM_{10} (2020). COD> 0.2 significant difference

APPENDIX B.

CONDITIONAL BIVARIATE PROBABILITY FUNCTION (CBPF) PLOTS

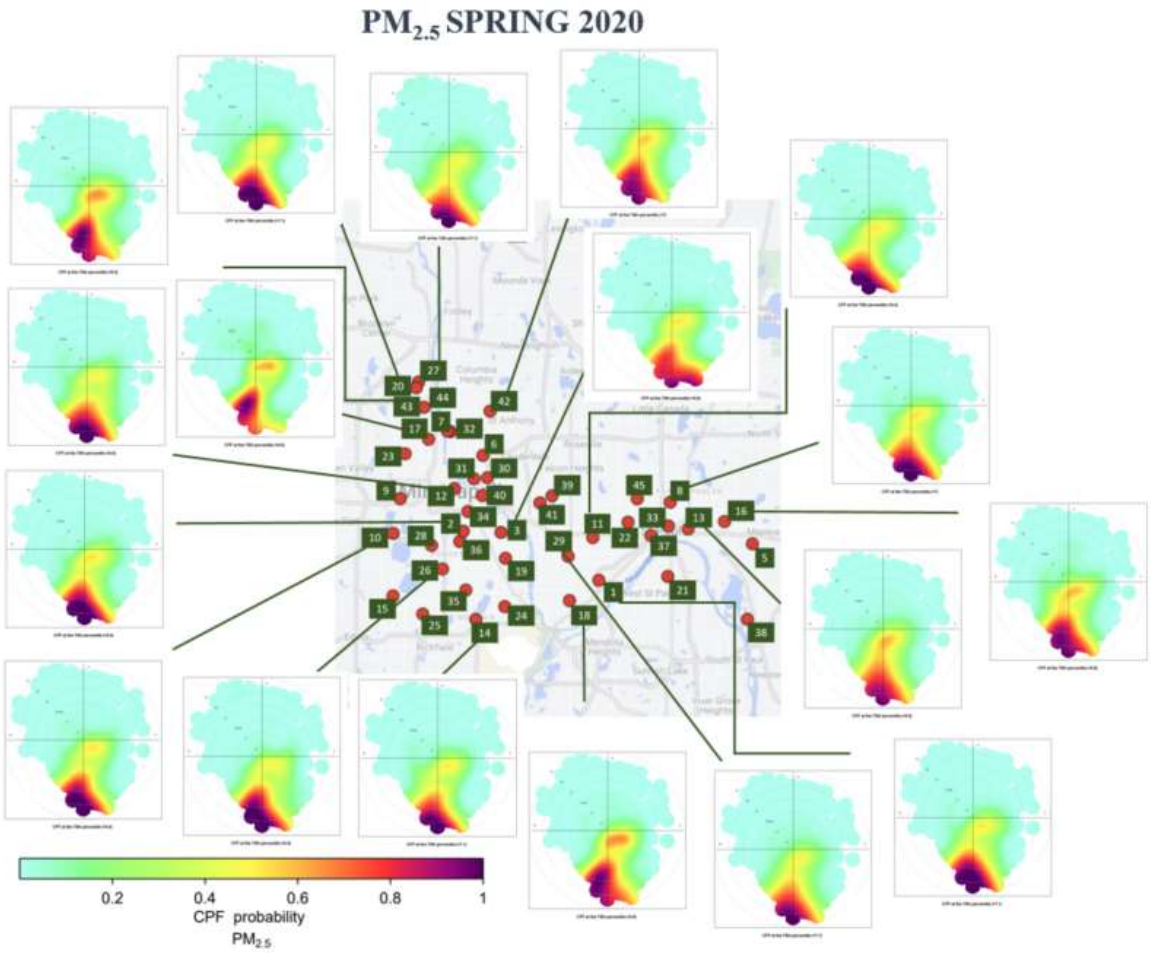

Figure B.1. CBPF plots for a 75th percentile threshold of $PM_{2.5}$ Concentration SP20

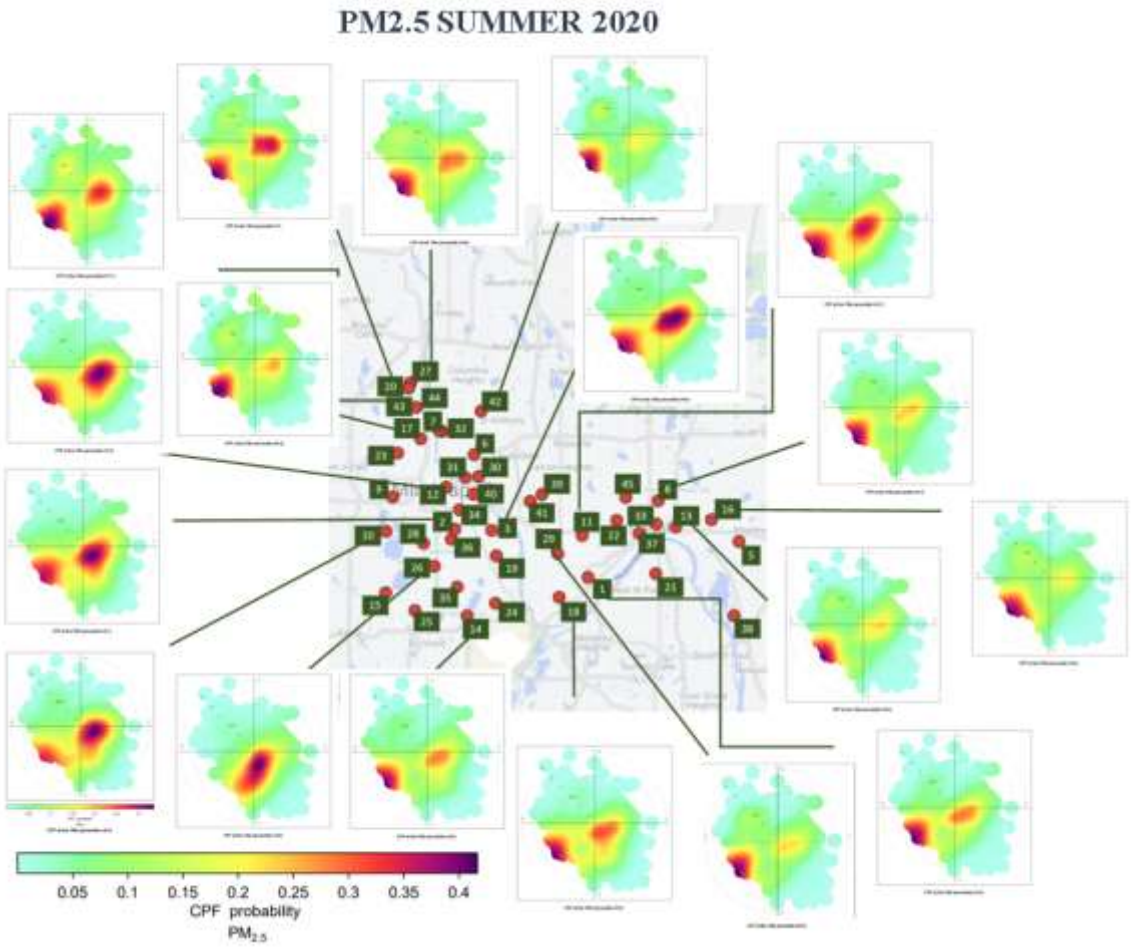

Figure B.2. CBPF plots for a 75th percentile threshold of $PM_{2.5}$ Concentration SM20

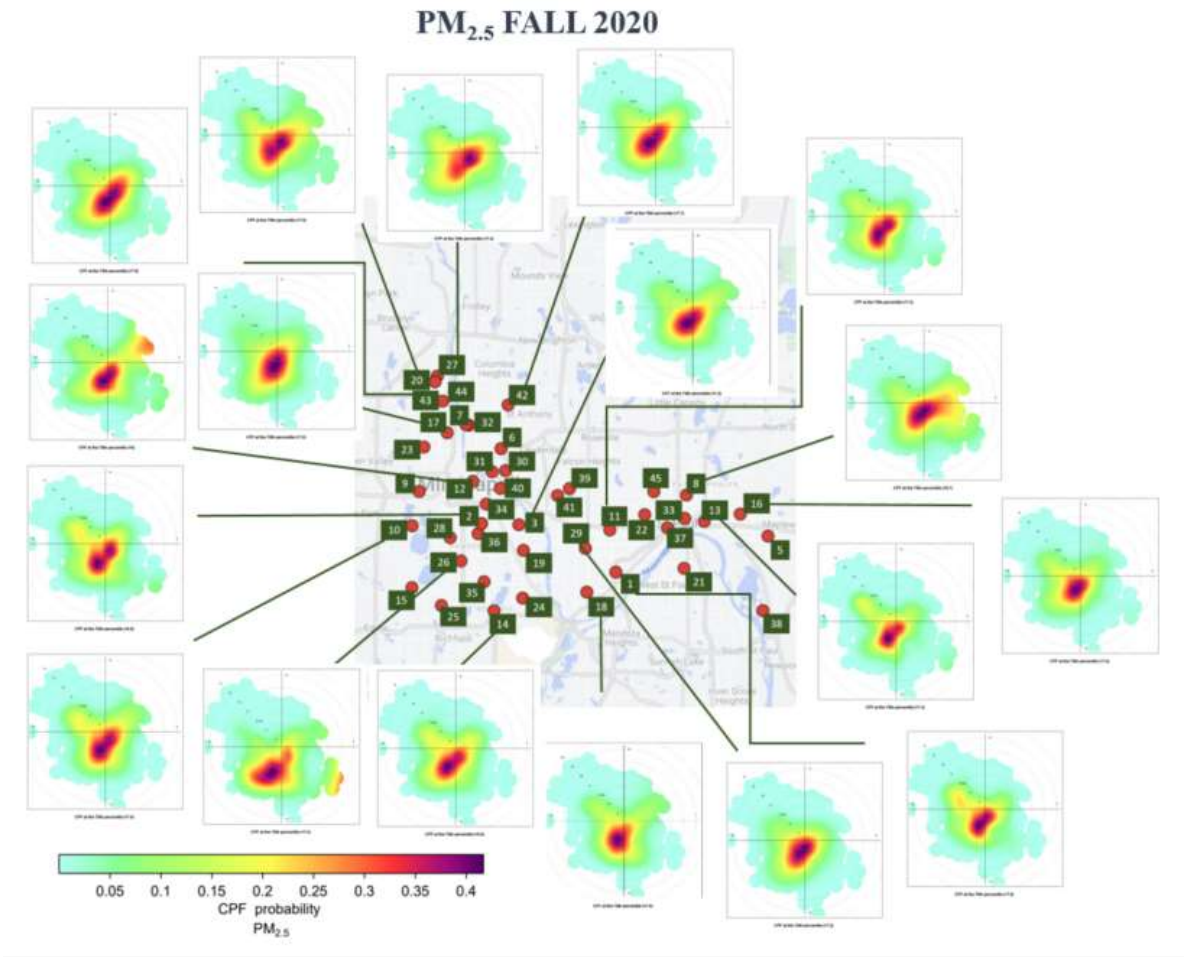

Figure B.3. CBPF plots for a 75th percentile threshold of $PM_{2.5}$ Concentration FL20

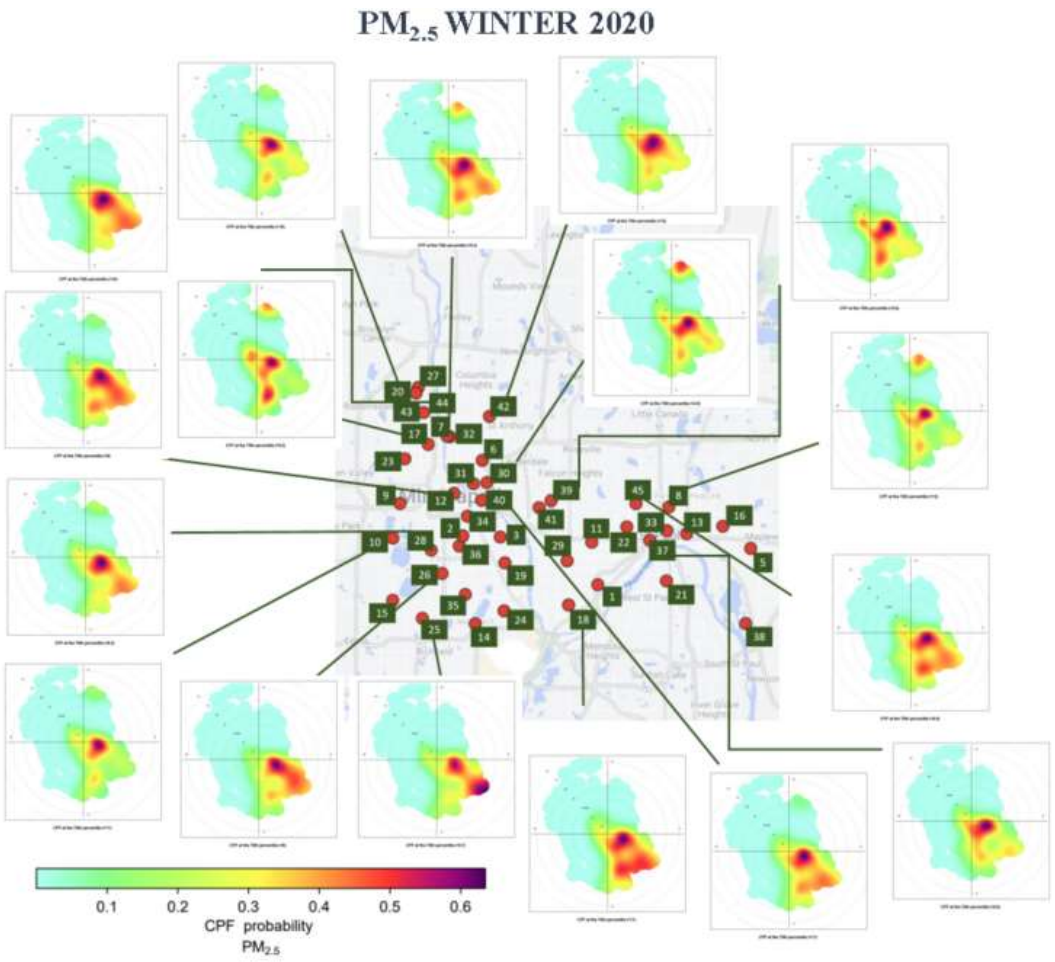

Figure B.4. CBPF plots for a 75th percentile threshold of $PM_{2.5}$ Concentration WN20

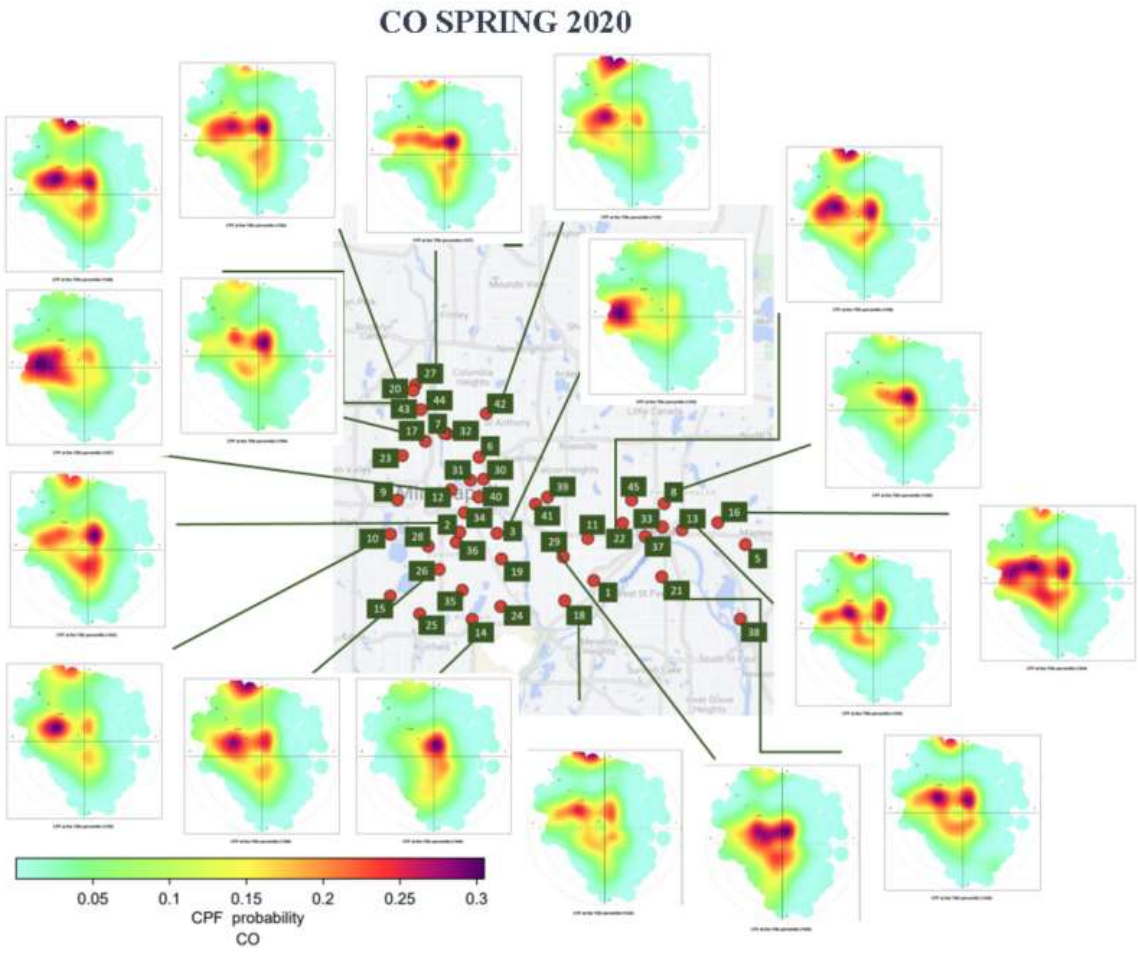

Figure B.5. CBPF plots for a 75th percentile threshold of CO Concentration SP20

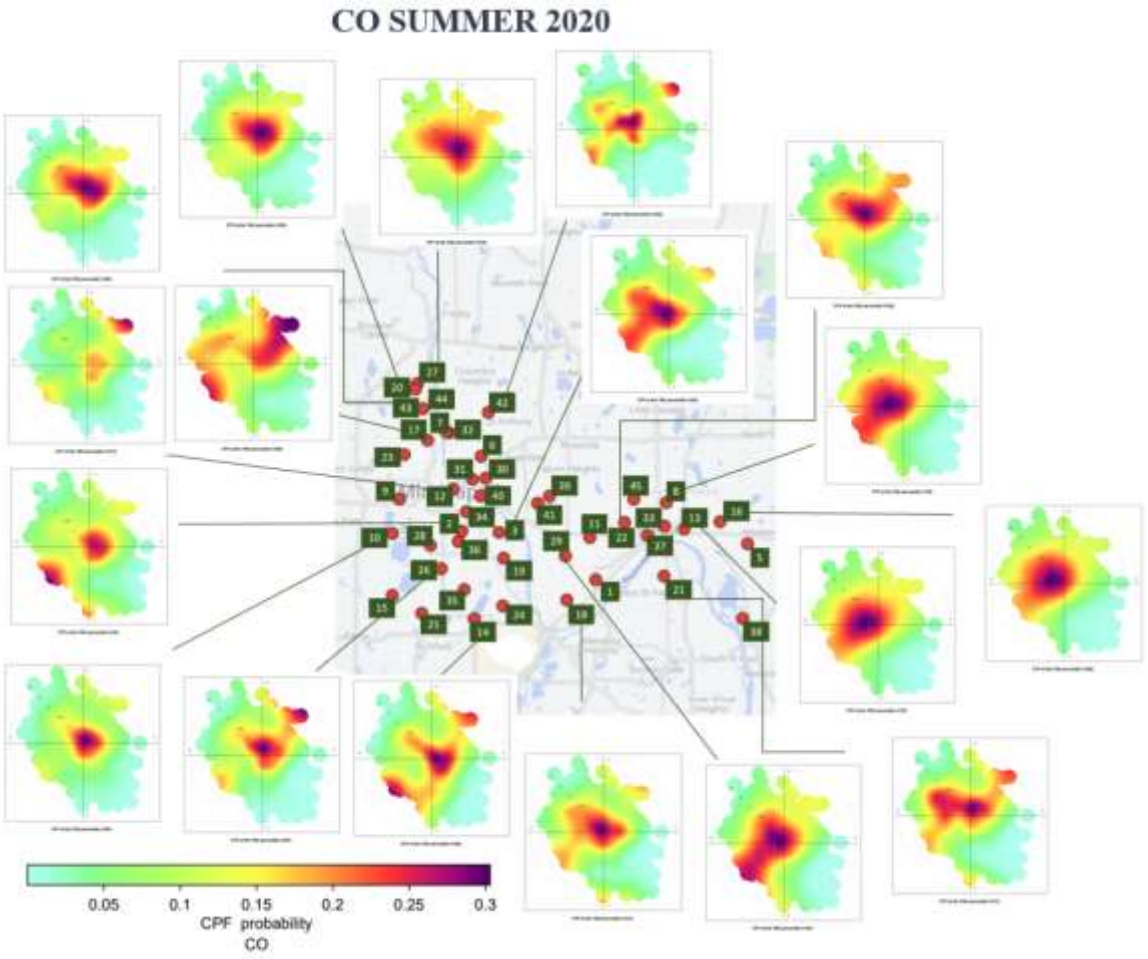

Figure B.6. CBPF plots for a 75th percentile threshold of CO Concentration SM20

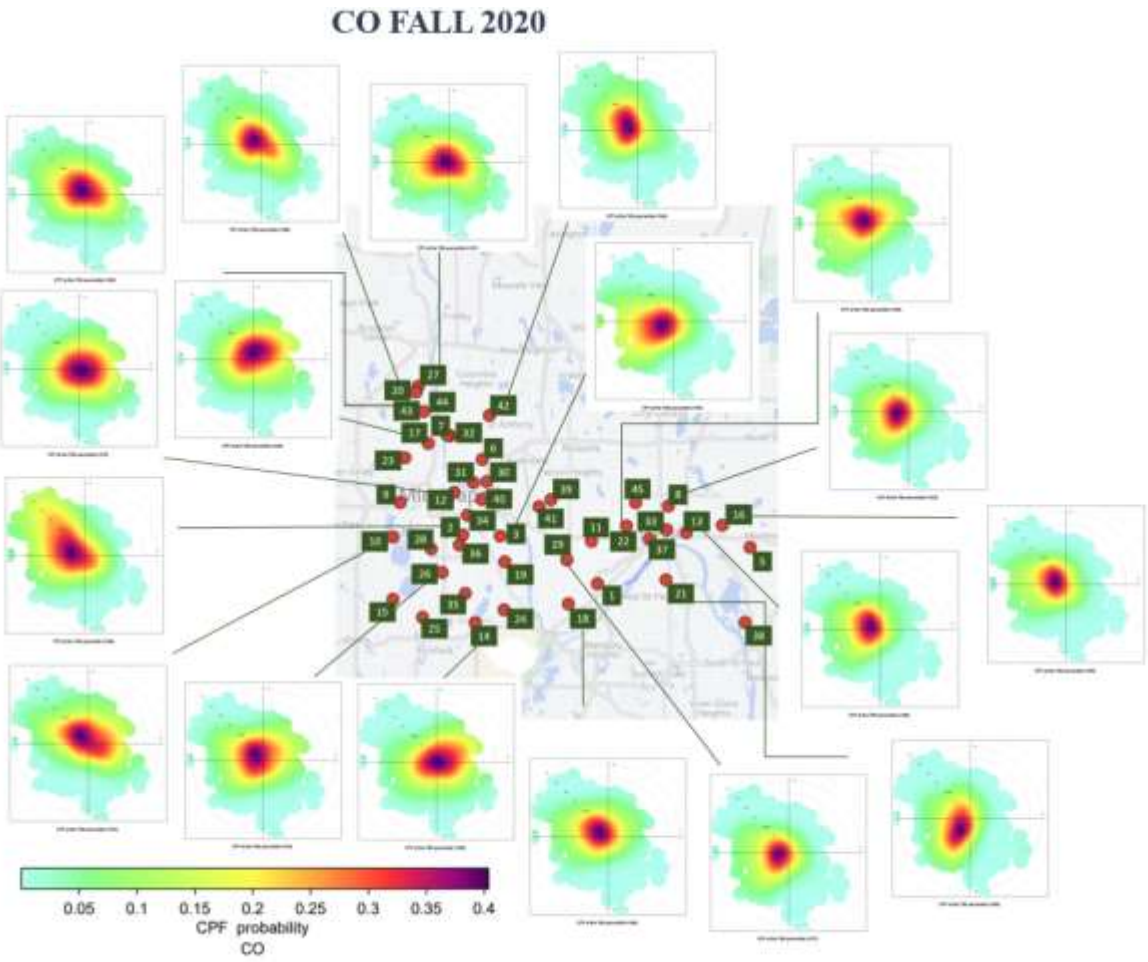

Figure B.7. CBPF plots for a 75th percentile threshold of CO Concentration FL20

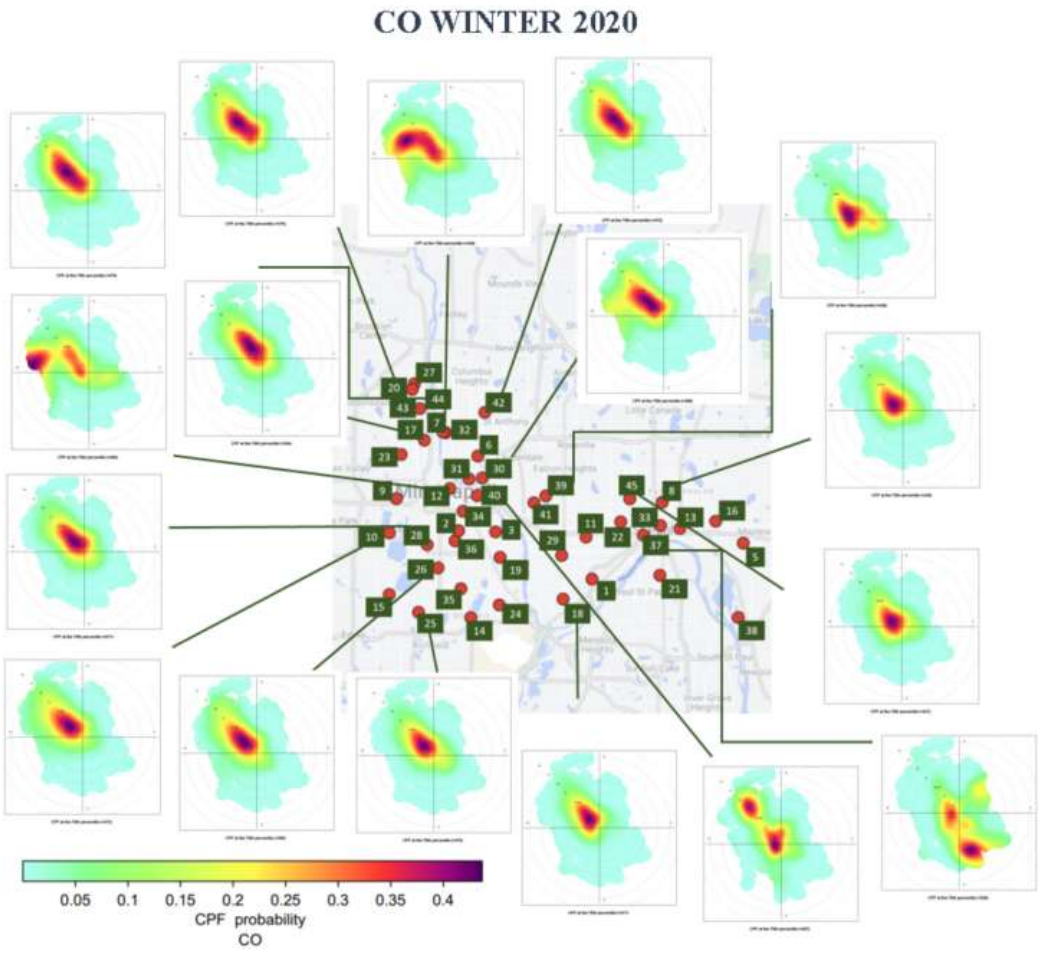

Figure B.8. CBPF plots for a 75th percentile threshold of CO Concentration WN20

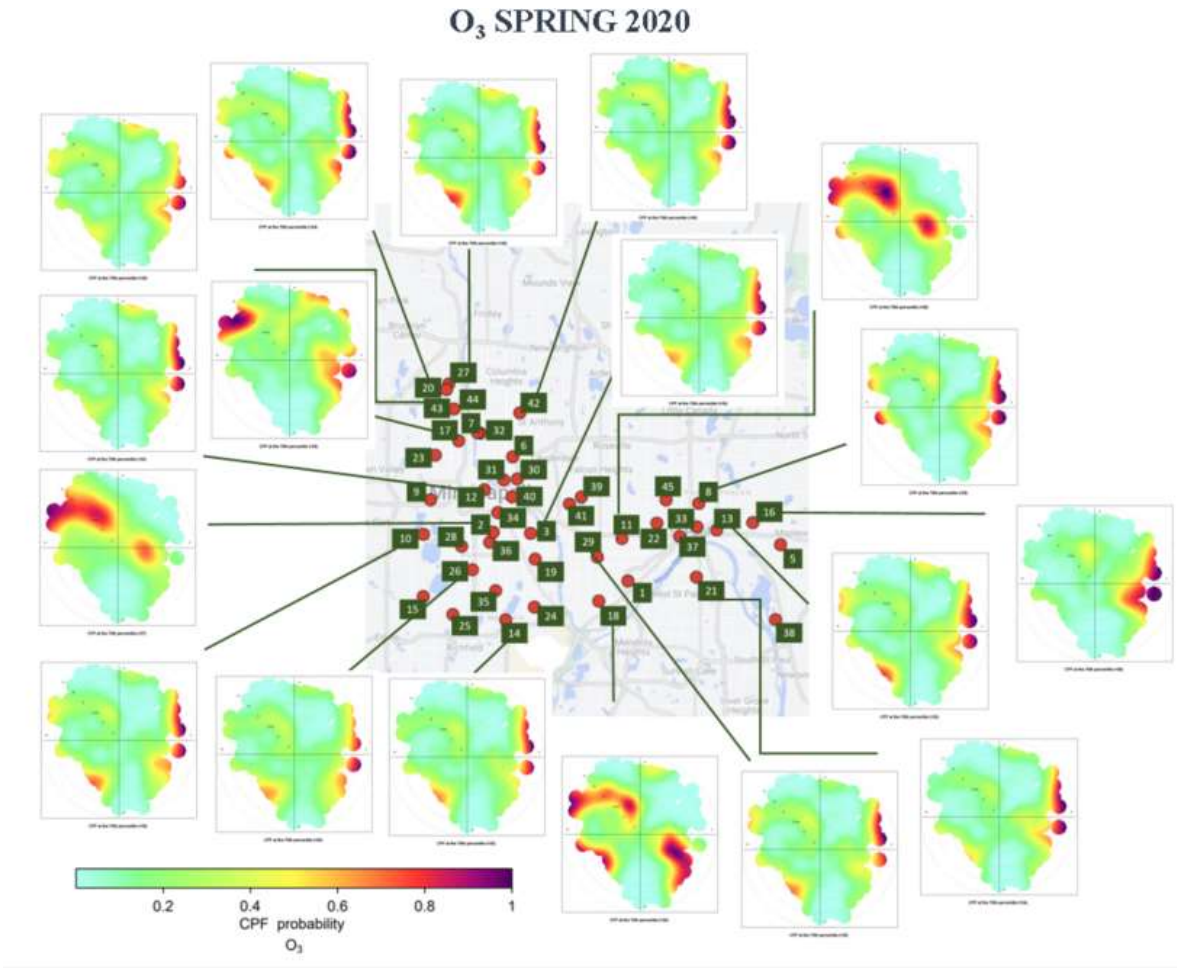

Figure B.9. CBPF plots for a 75th percentile threshold of O_3 Concentration SP20

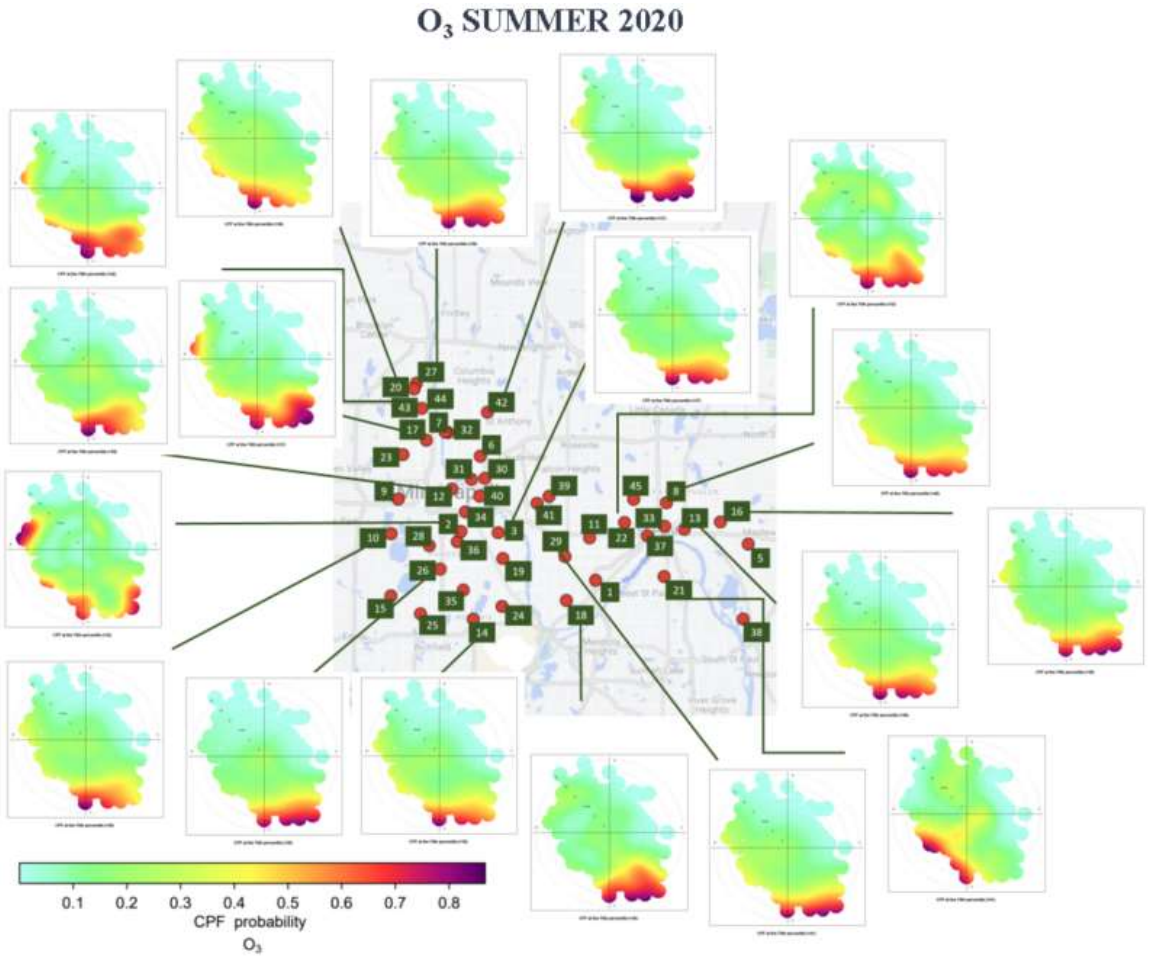

Figure B.10. CBPF plots for a 75th percentile threshold of O_3 Concentration SM20

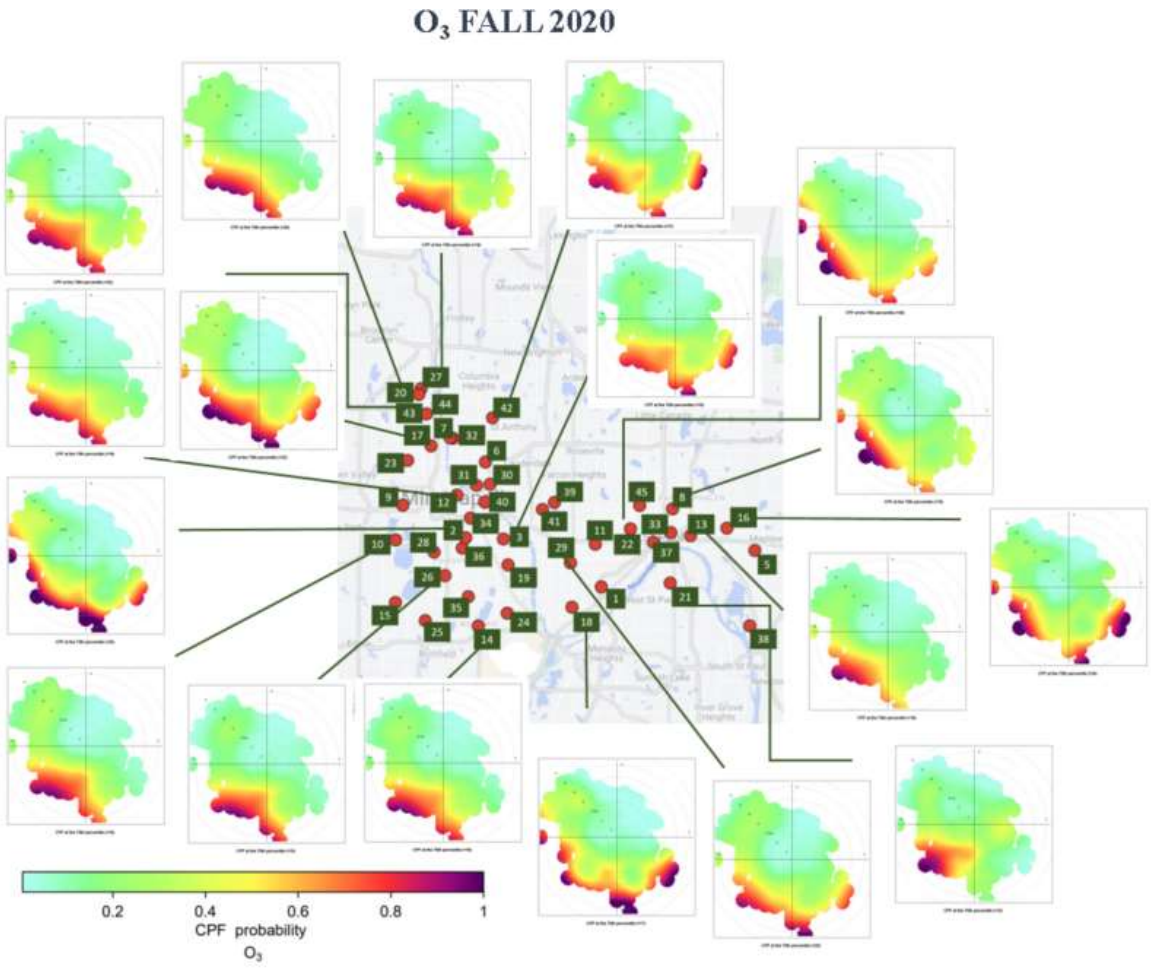

Figure B.11. CBPF plots for a 75th percentile threshold of O_3 Concentration FL20

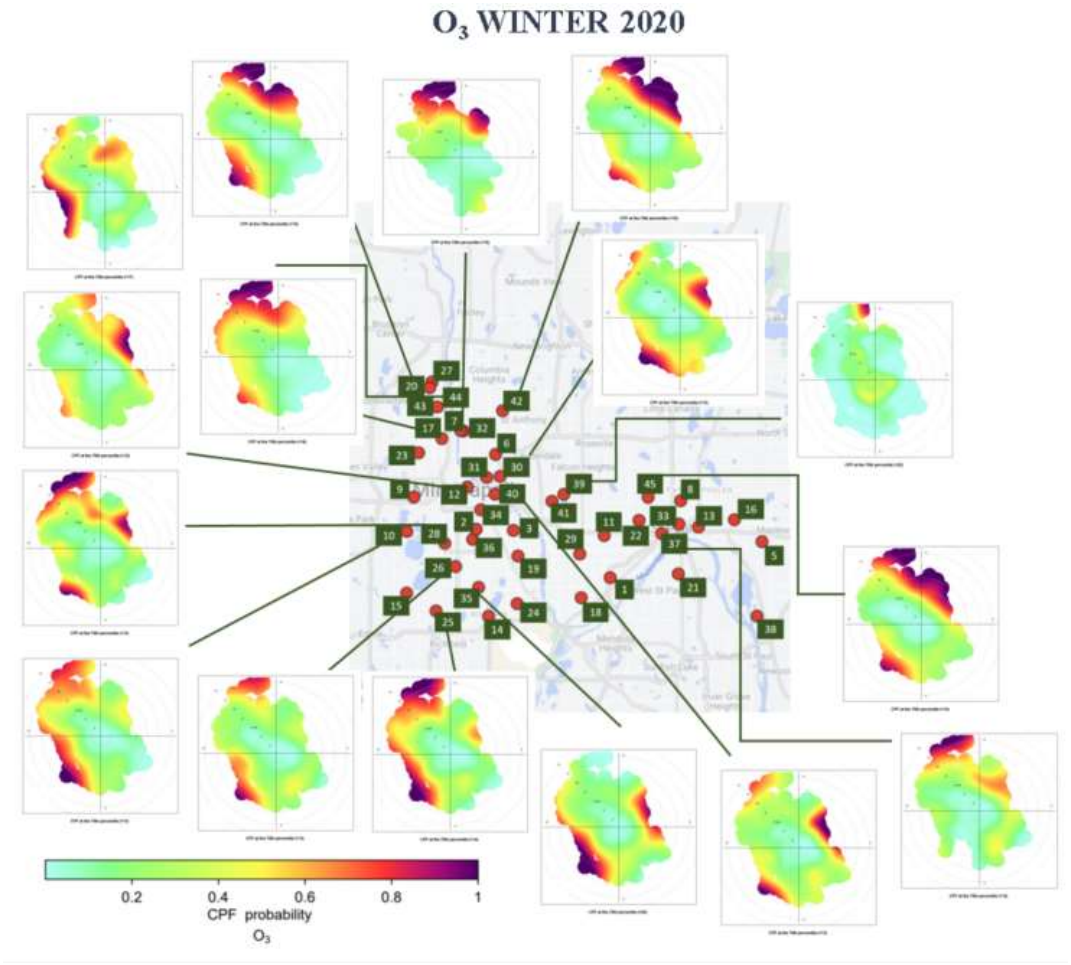

Figure B.12. CBPF plots for a 75th percentile threshold of O_3Concentration WN20

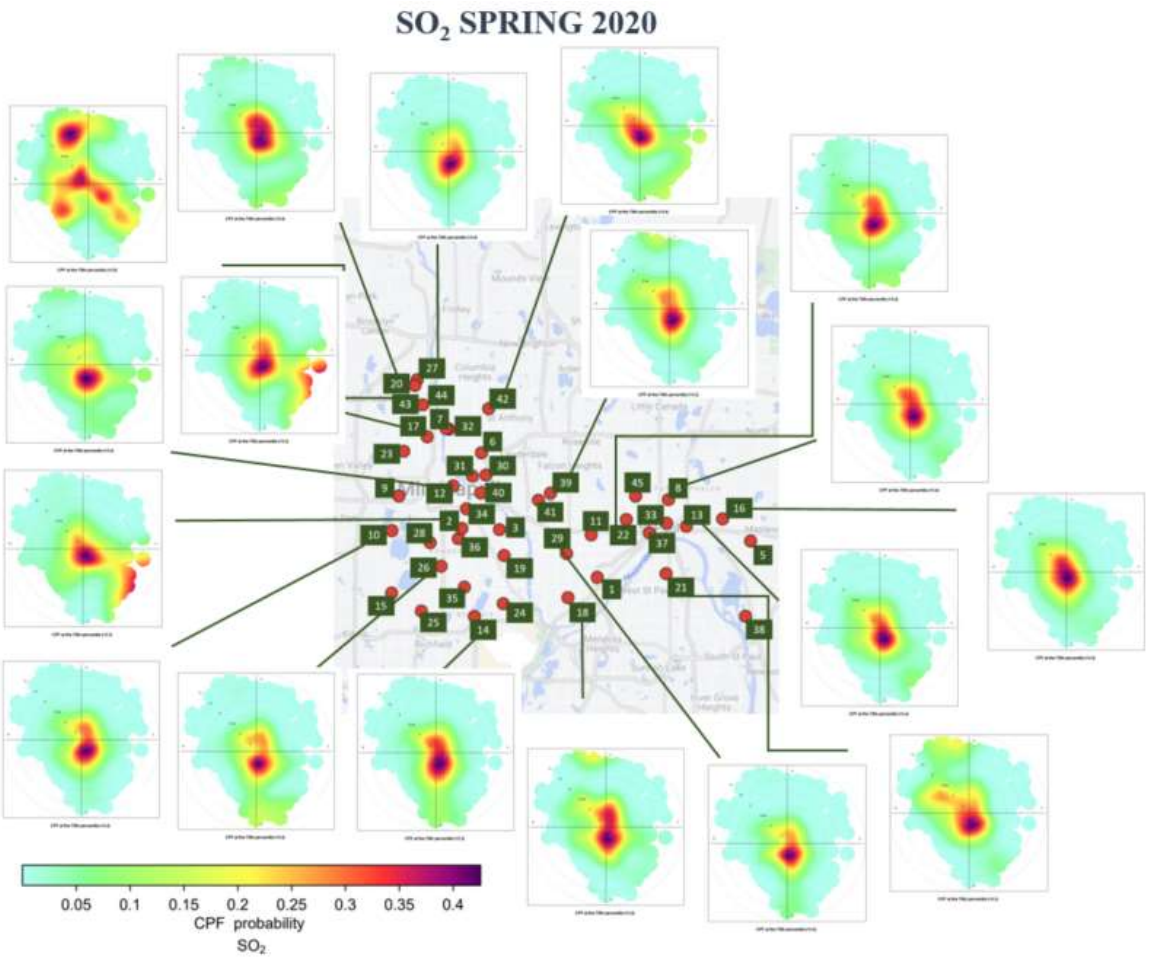

Figure B.13. CBPF plots for a 75th percentile threshold of SO_2 Concentration SP20

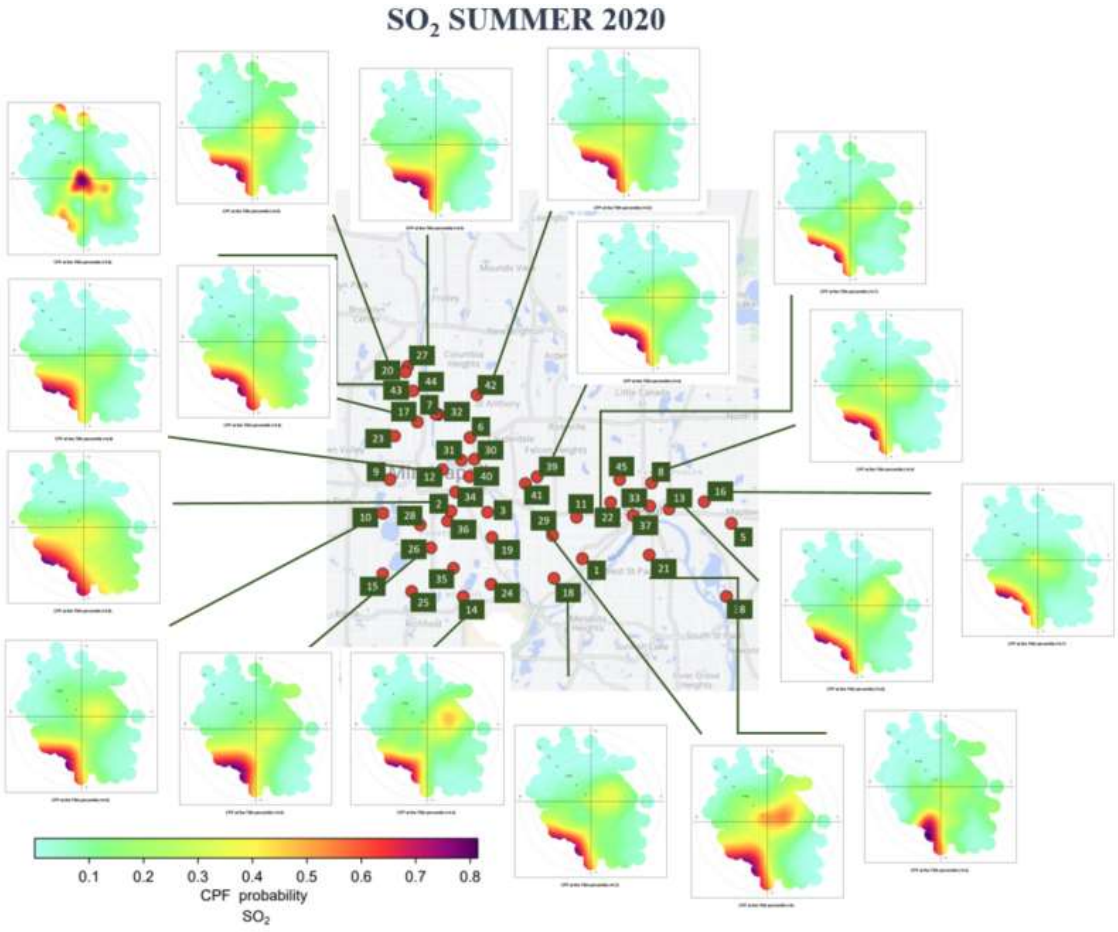

Figure B.14. CBPF plots for a 75th percentile threshold of SO_2 Concentration SM20

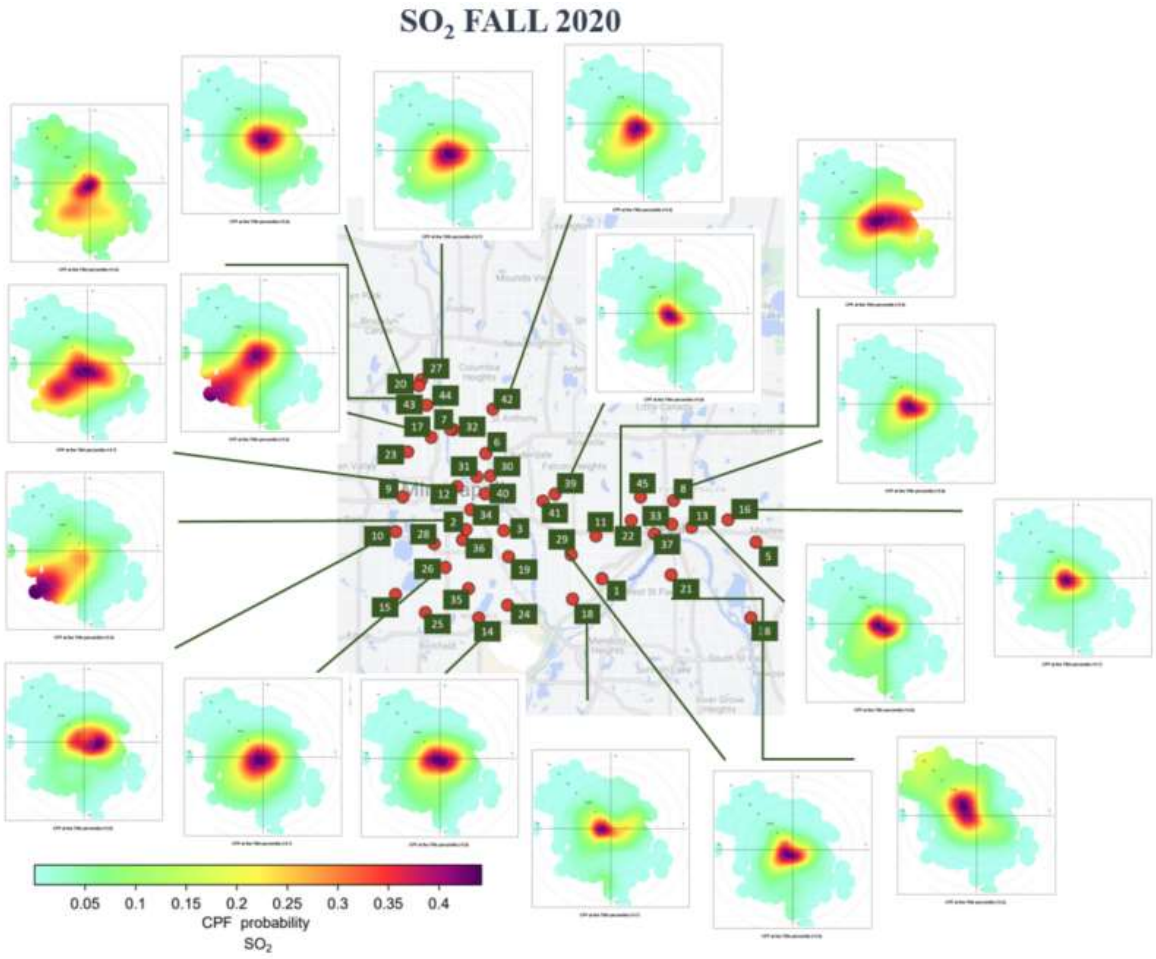

Figure B.15. CBPF plots for a 75th percentile threshold of SO_2 Concentration FL20

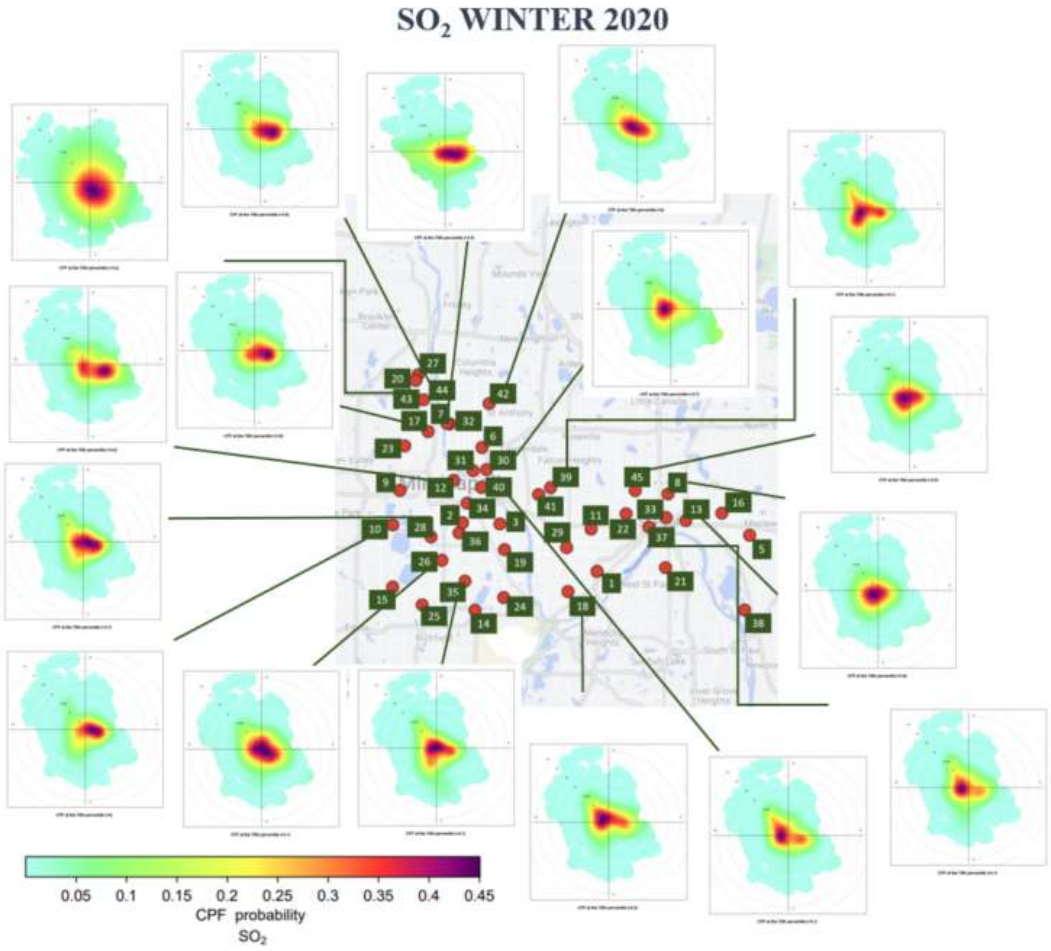

Figure B.16. CBPF plots for a 75th percentile threshold of SO_2 Concentration WN20

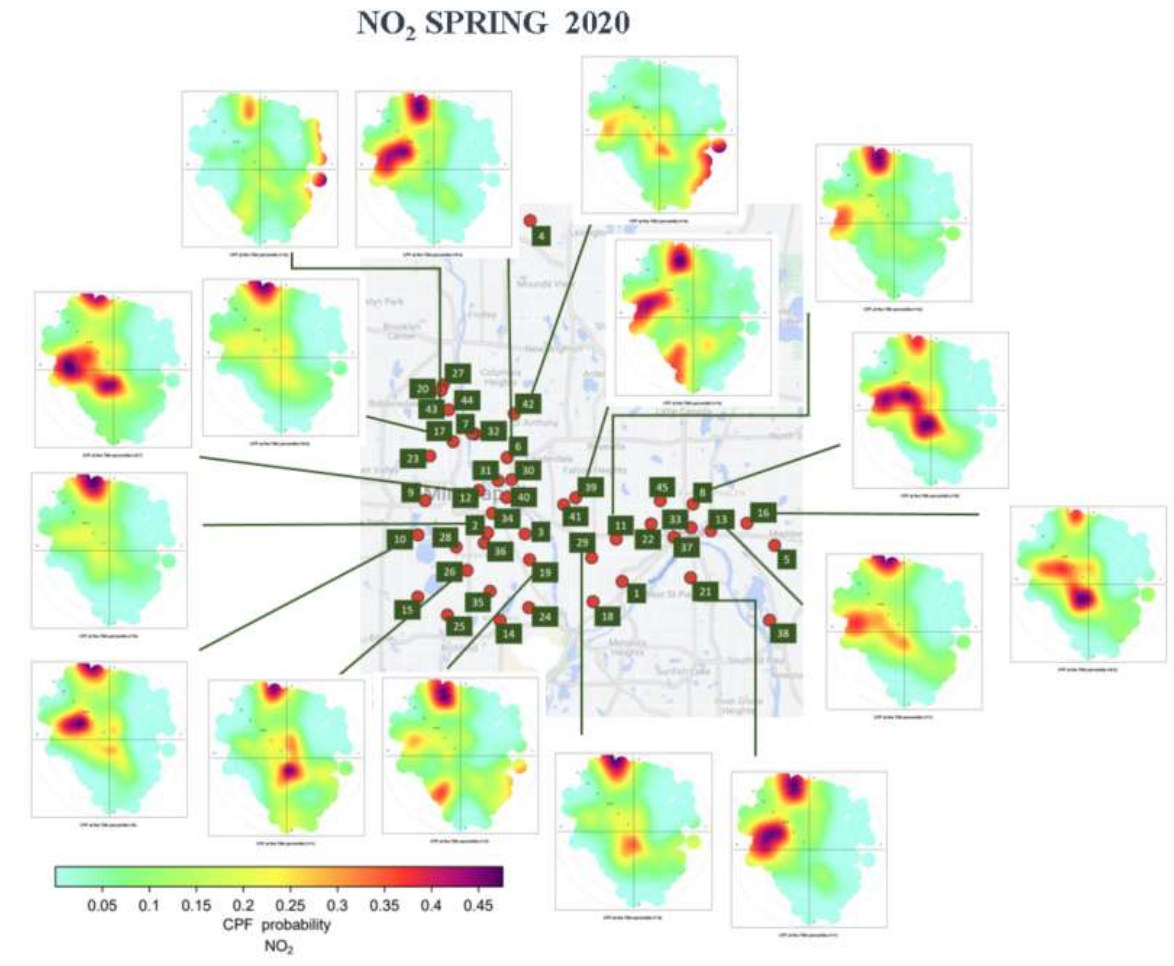

Figure B.17. CBPF plots for a 75th percentile threshold of NO_2 Concentration SP20

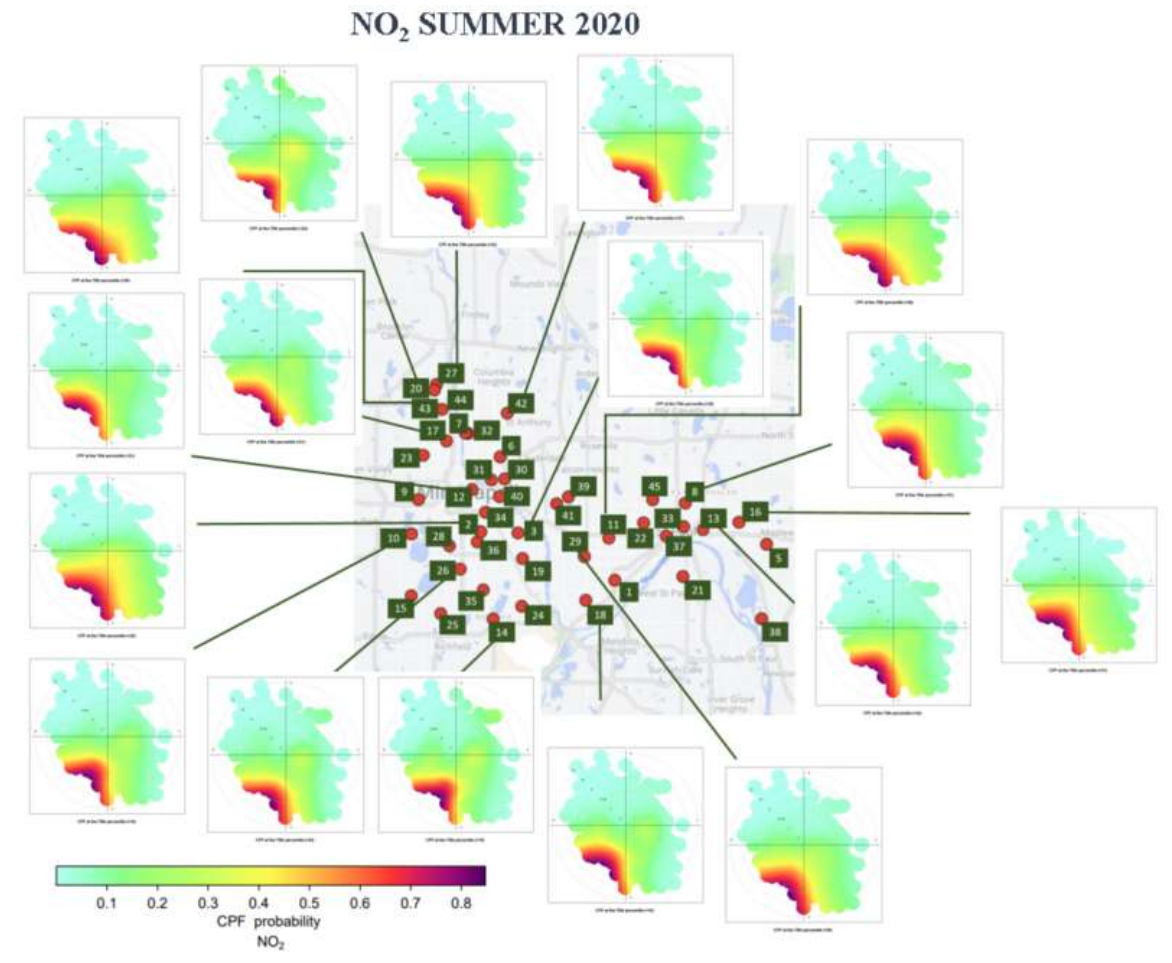

Figure B.18. CBPF plots for a 75th percentile threshold of NO_2 Concentration SM20

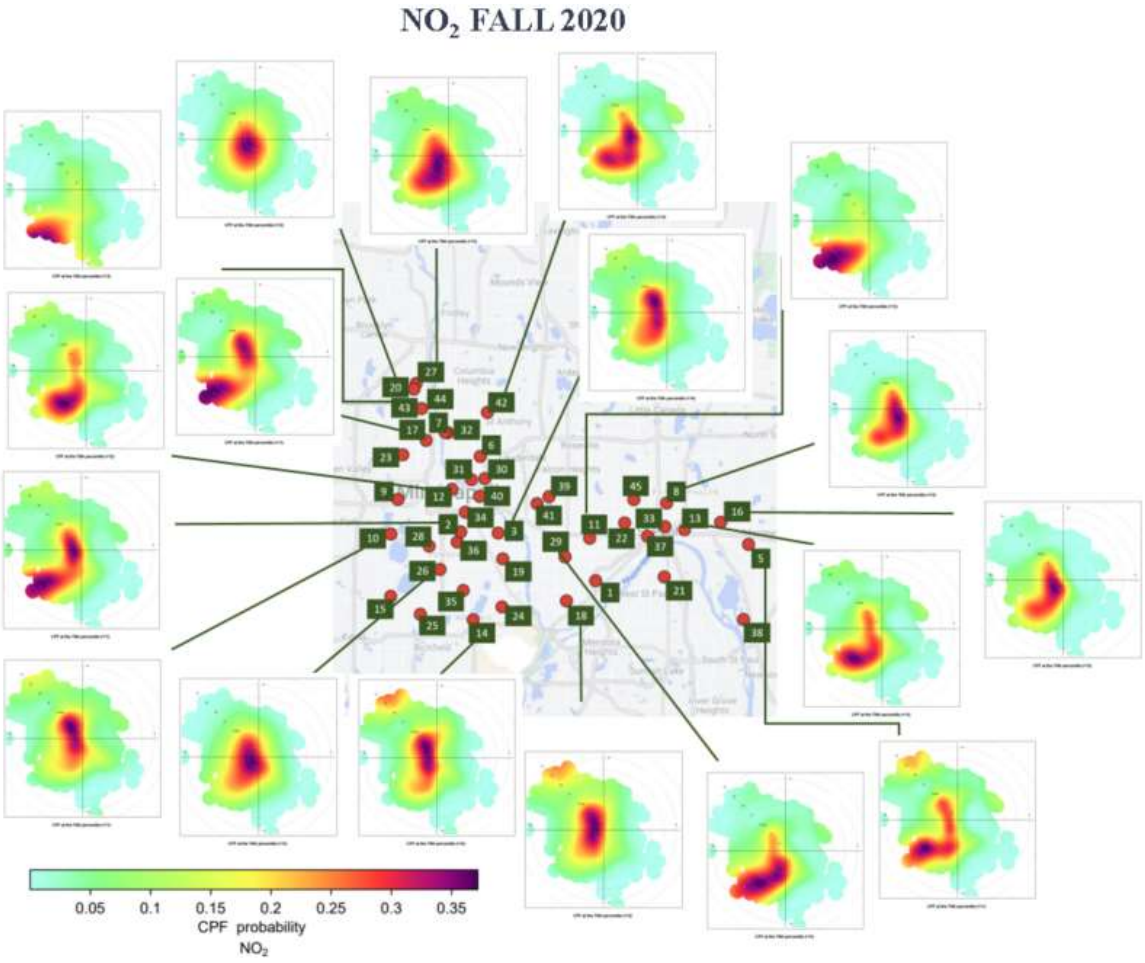

Figure B.19. CBPF plots for a 75th percentile threshold of NO_2 Concentration FL20

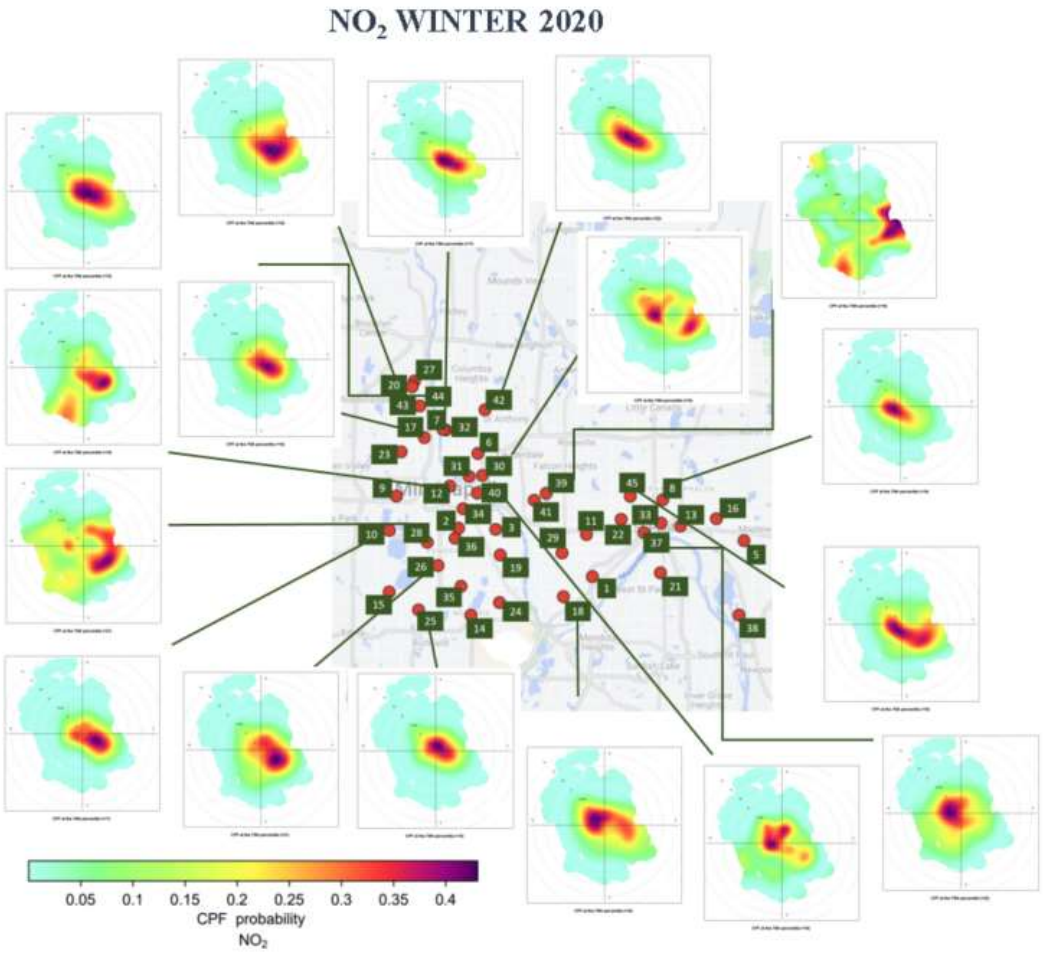

Figure B.20. CBPF plots for a 75th percentile threshold of NO_2 Concentration WN20

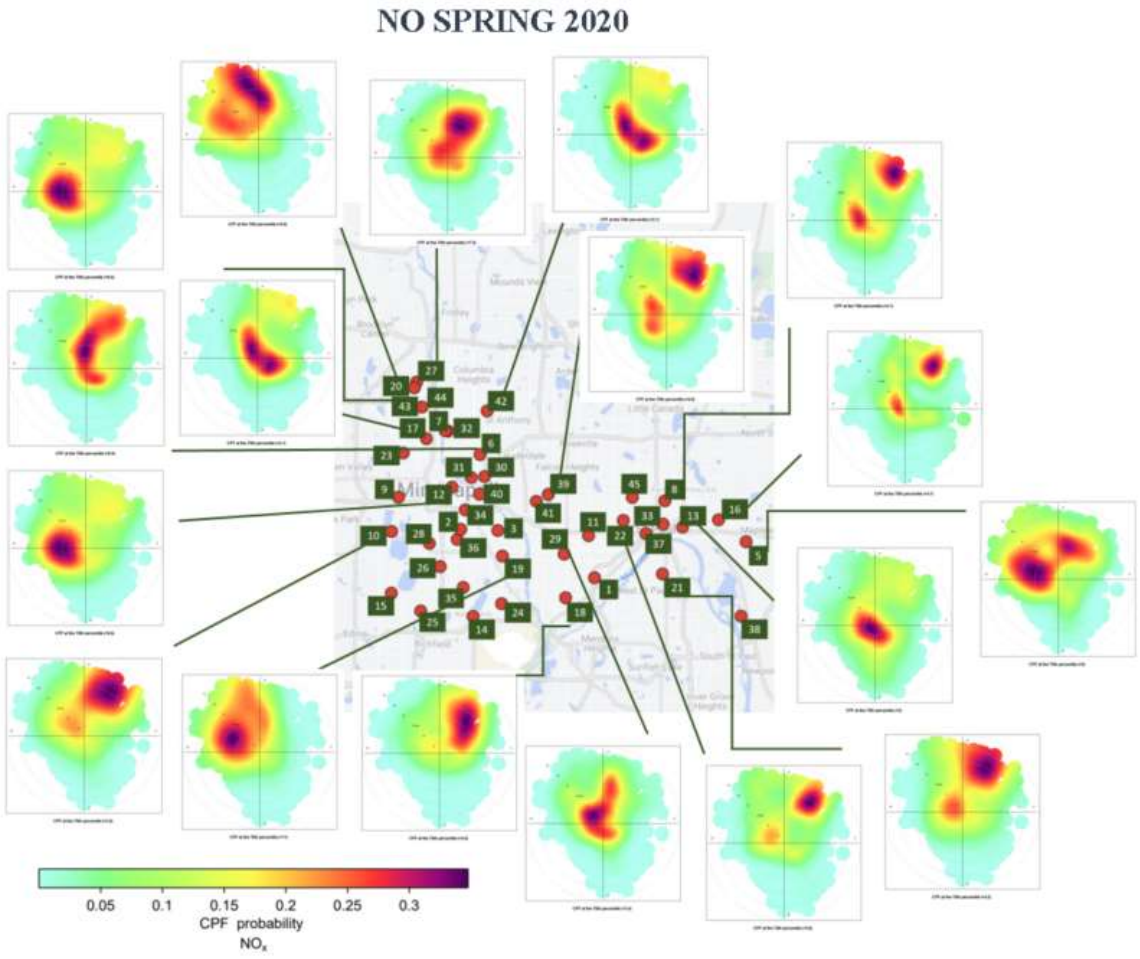

Figure B.21. CBPF plots for a 75th percentile threshold of NO Concentration SP20

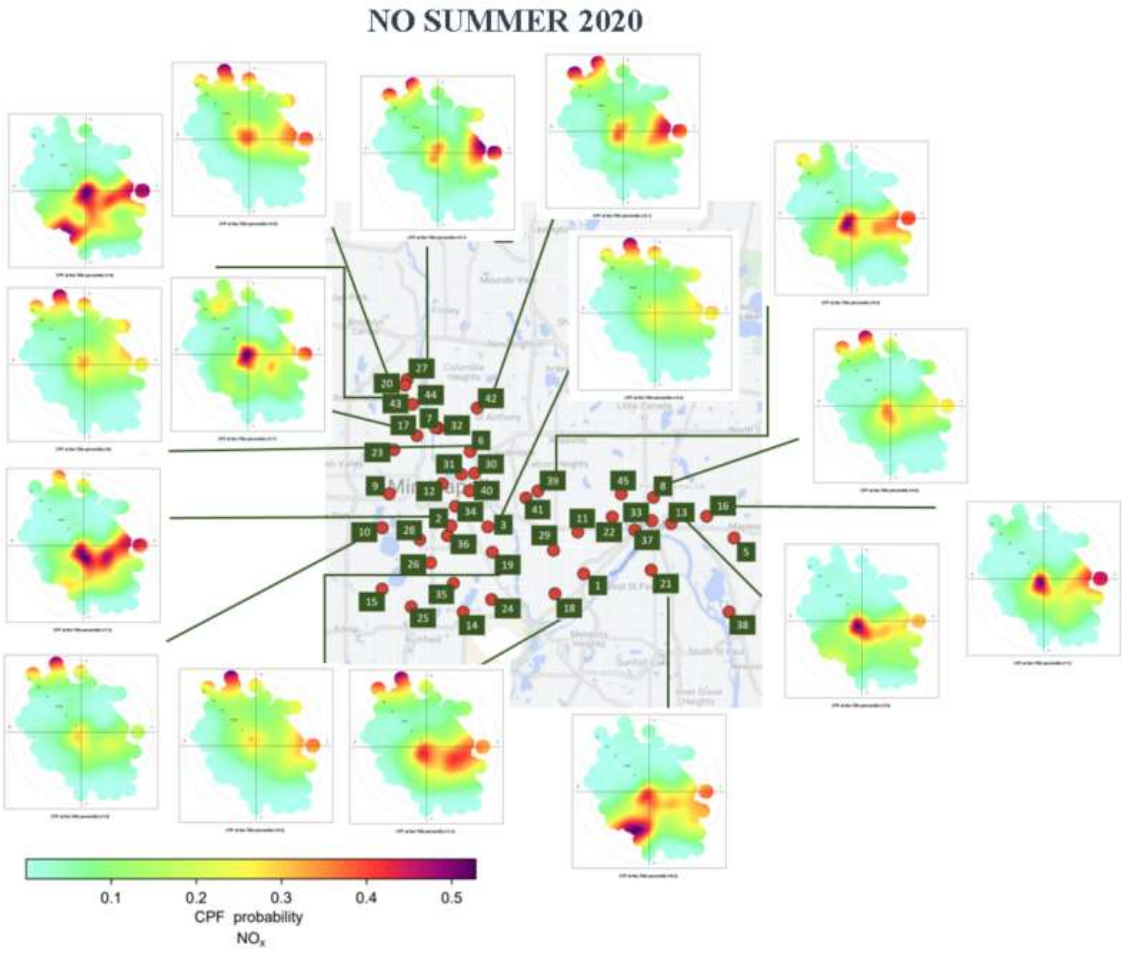

Figure B.22. CBPF plots for a 75th percentile threshold of NO Concentration SM20

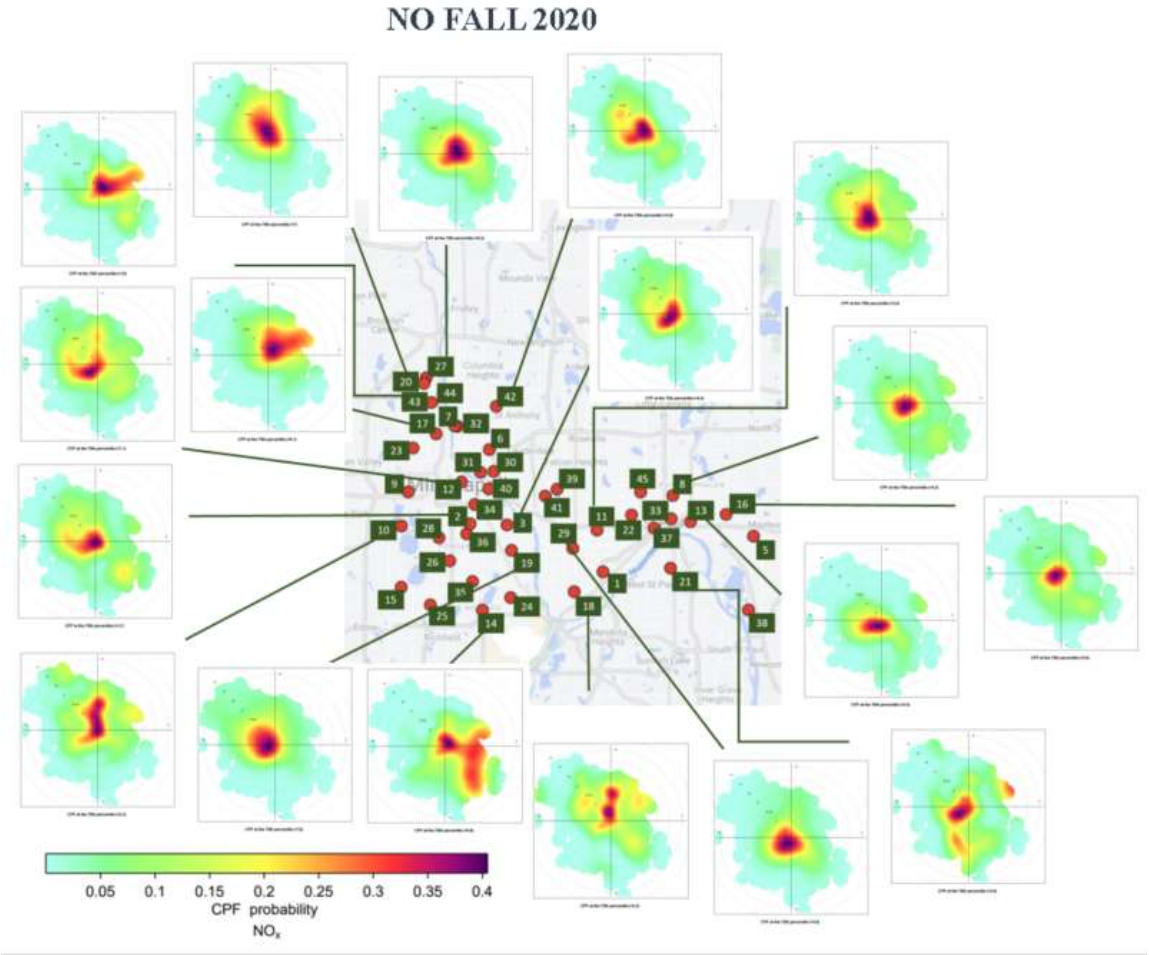

Figure B.23. CBPF plots for a 75th percentile threshold of NO Concentration FL20

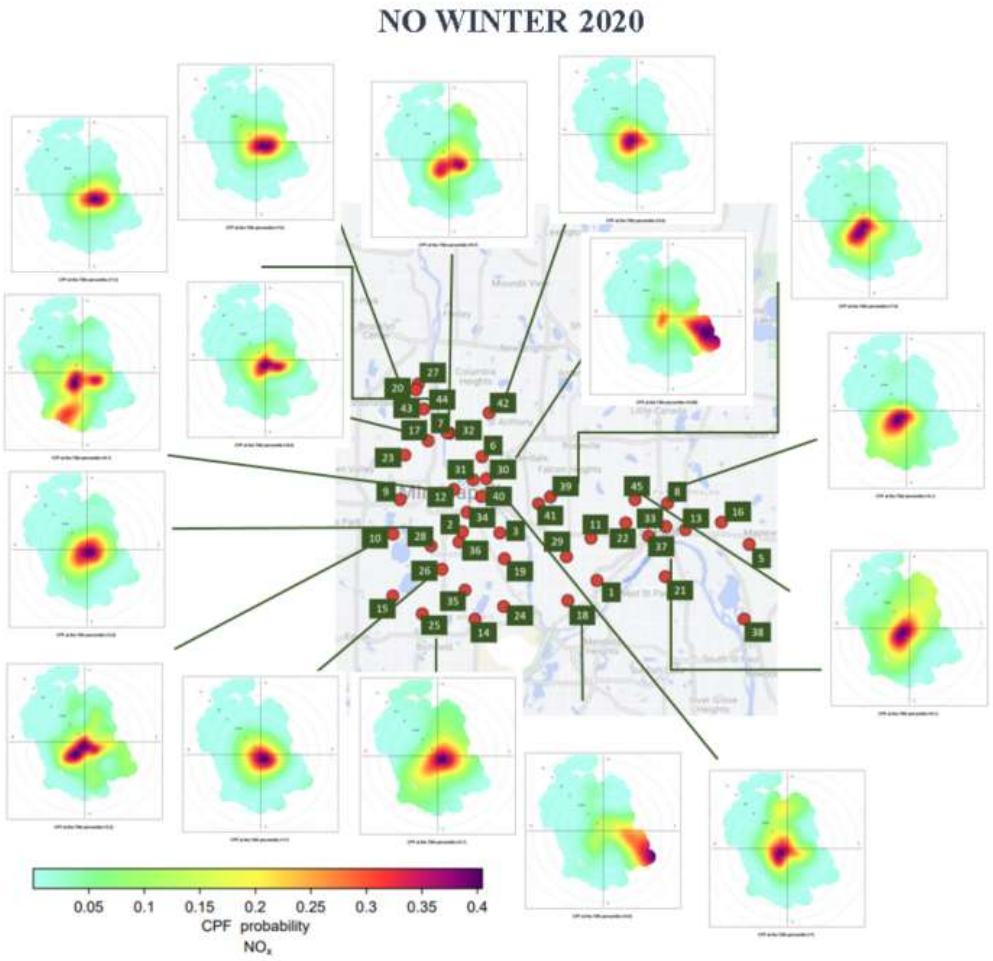

Figure B.24. CBPF plots for a 75th percentile threshold of NO Concentration WN20

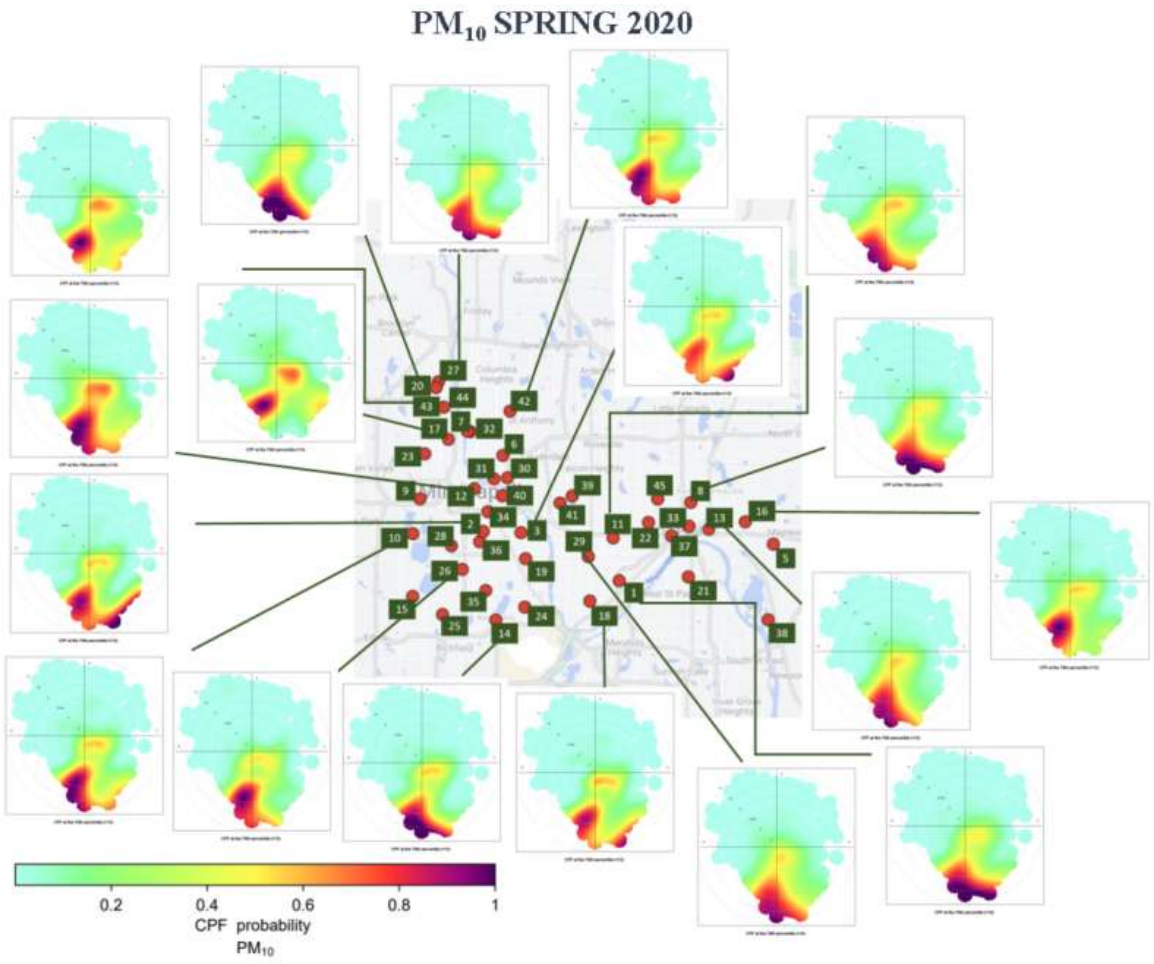

Figure B.25. CBPF plots for a 75th percentile threshold of PM_{10} Concentration SP20

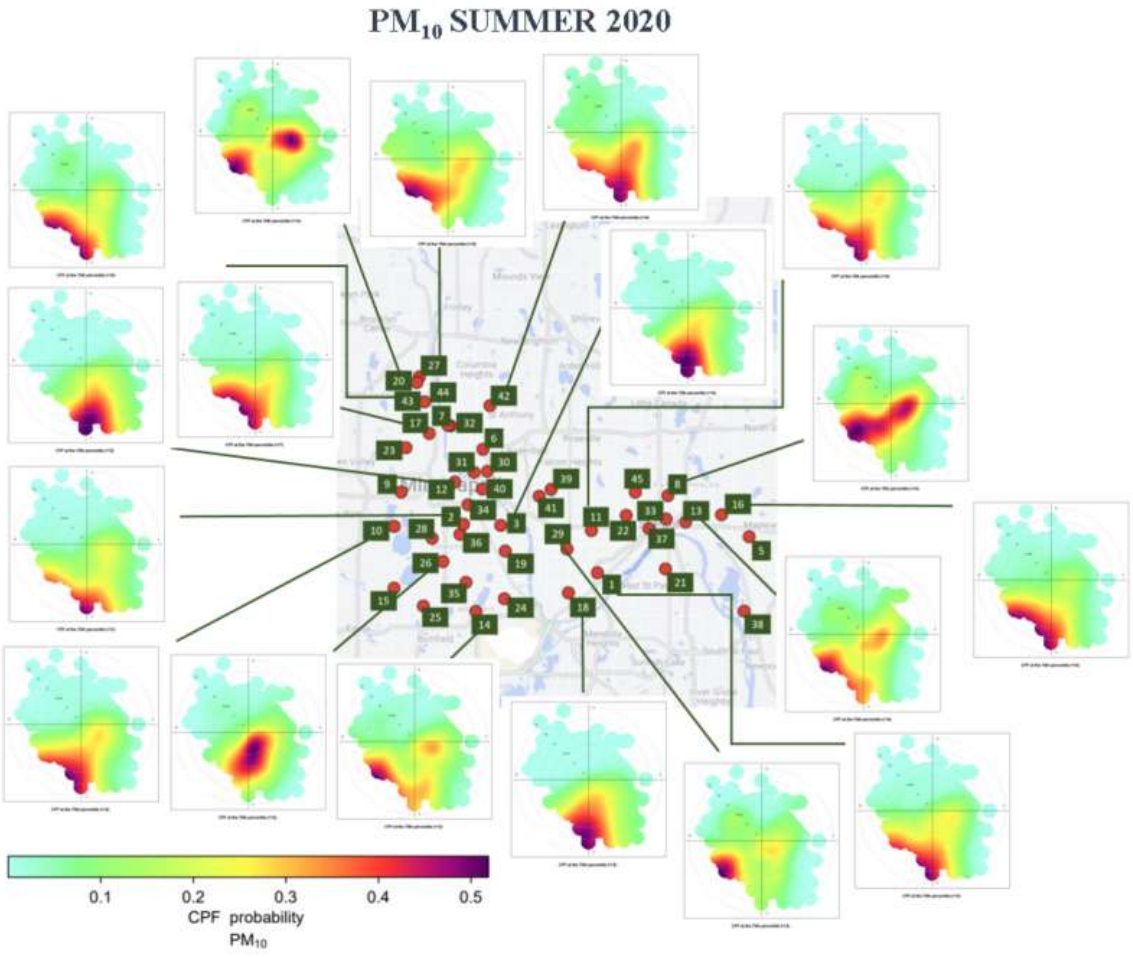

Figure B.26. CBPF plots for a 75th percentile threshold of PM_{10} Concentration SM20

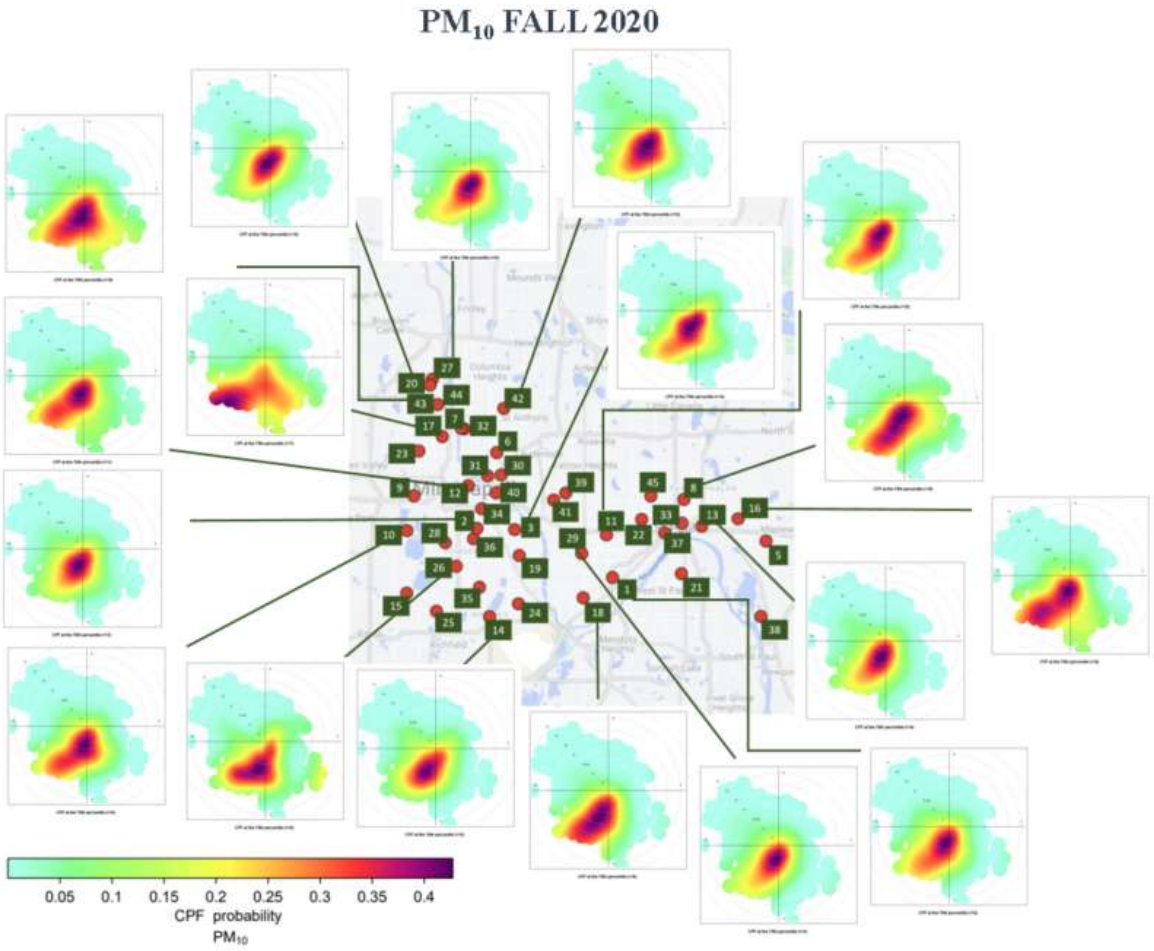

Figure B.27. CBPF plots for a 75th percentile threshold of PM_{10} Concentration FL20

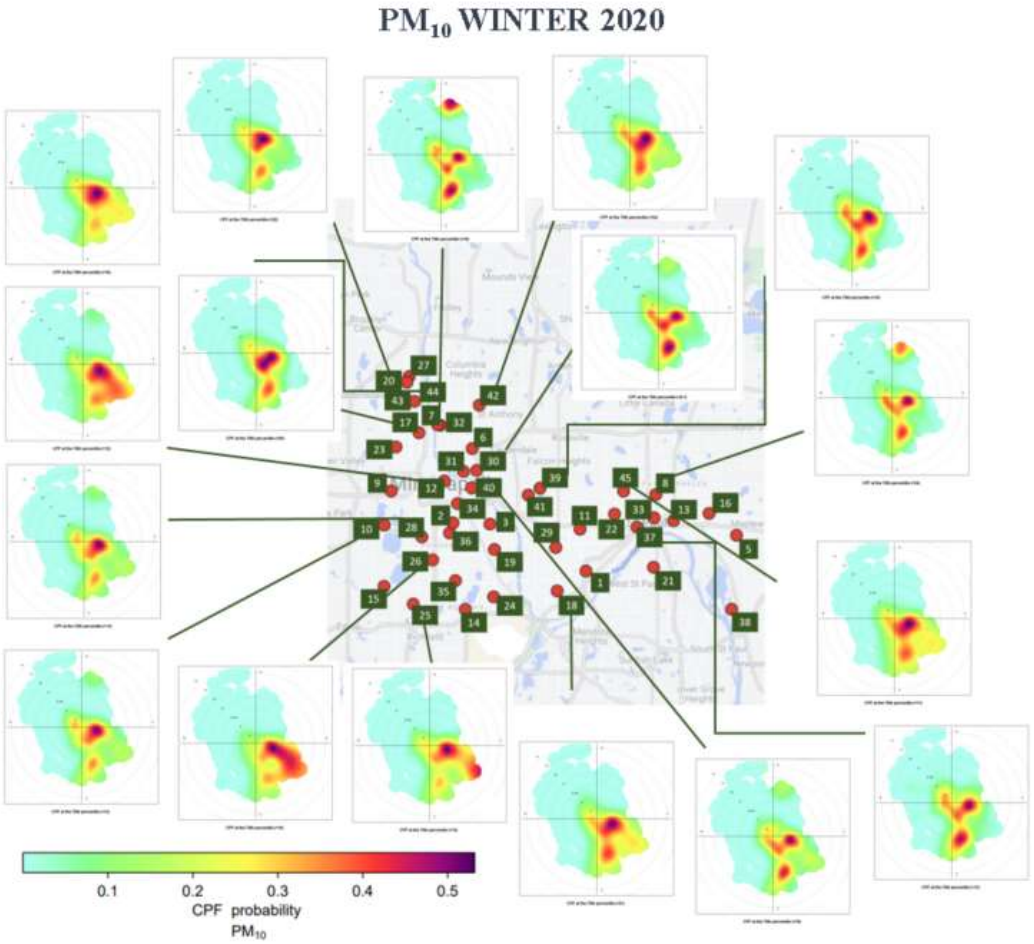

Figure B.28. CBPF plots for a 75th percentile threshold of PM_{10} Concentration WN20

BIBLIOGRAPHY

Aneja, V. P., Arya, S. P., Li, Y., Murray, G. C., Jr, & Manuszak, T. L. (2000). Climatology of diurnal trends and vertical distribution of ozone in the atmospheric boundary layer in urban North Carolina. Journal of the Air & Waste Management Association (1995), 50(1), 54–64. https://doi.org/10.1080/10473289.2000.10463984

Ashbaugh, Lowell L., William C. Malm, and Willy Z. Sadeh. (1985). "A residence time probability analysis of sulfur concentrations at grand Canyon National Park." Atmospheric Environment (1967) 19 (8): 1263–70. https://doi.org/10.1016/0004-6981(85)90256-2.

Bi, J., Zuidema, C., Clausen, D., Kirwa, K., Young, M. T., Gassett, A. J., ... & Kaufman, J. D. (2022). Within-City Variation in Ambient Carbon Monoxide Concentrations: Leveraging Low-Cost Monitors in a Spatiotemporal Modeling Framework. Environmental Health Perspectives, 130(9), 097008.

Carslaw, D. C., and K. Ropkins. (2012). Openair — An R package for air quality data analysis. Environmental Modelling & Software 27–28 (0): 52–61. https://doi.org/10.1016/j.envsoft.2011.09.008.

Clements, A., & Vanderpool, R. (2019, December 18). FRMs/FEMs and Sensors: Complementary Approaches for Determining Ambient Air Quality [Webinar]. US EPA Office of Research and Development. https://www.epa.gov/sites/default/files/2019-12/documents/frm-fem_and_air_sensors_dec_2019_webinar_slides_508_compliant.pdf

Health Effects Institute. 2020. State of Global Air 2020. Special Report. Boston, MA: Health Effects Institute. https://www.stateofglobalair.org/

Jayaratne, R., Thai, P., Christensen, B., Liu, X., Zing, I., Lamont, R., Dunbabin, M., Dawkins, L., Bertrand, L., & Morawska, L. (2021). The effect of cold-start emissions on the diurnal variation of carbon monoxide concentration in a city centre. Atmospheric environment, 245, 118035. doi:10.1016/j.atmosenv.2020.118035

Jiao, W., Hagler, G., Williams, R., Sharpe, R., Brown, R., Garver, D., Judge, R., Caudill, M., Rickard, J., Davis, M., Weinstock, L., Zimmer-Dauphinee, S., & Buckley, K. (2016). Community Air Sensor Network (CAIRSENSE) project: evaluation of low-cost sensor performance in a suburban environment in the southeastern United States. Atmospheric measurement techniques, 9(11), 5281–5292. https://doi.org/10.5194/amt-9-5281-2016

Kendrick, C.M., Koonce, P., George, L.A., Diurnal and seasonal variations of NO, NO2 and PM2.5 mass as a function of traffic volumes alongside an urban arterial, Atmospheric Environment (2015), doi: 10.1016/j.atmosenv.2015.09.019

Krudysz, M., Moore, K., Geller, M., Sioutas, C., and Froines, J. (2009). Intra-community spatial variability of particulate matter size distributions in Southern California/Los Angeles.Atmos. Chem. Phys., 9, 1061–1075, https://doi.org/10.5194/acp-9-1061-2009, 2009

Kumar, P., Morawska, L., Martani, C., Biskos,G., Neophytou, M., Sabatino, S.D., Bell,M., Norford, L., & Britter, R. (2014). The rise of low-cost sensing for managing air pollution in cities. Environment International. https://doi.org/10.1016/j.envint.2014.11.019.

Lane, H. M., Morello-Frosch, R., Marshall, J. D., & Apte, J. S. (2022). Historical Redlining is Associated with Present-Day Air Pollution Disparities in U.S. Cities. Environmental science & technology letters, 9(4), 345–350. https://doi.org/10.1021/acs.estlett.1c01012

Lazaridis, Mihalis & Latos, M. & Aleksandropoulou, Victoria & Hov, Øystein & Papayannis, Alex & Tørseth, Kjetil. (2008). Contribution of forest fire emissions to atmospheric pollution in Greece. Air Quality, Atmosphere & Health. 1. 143-158. 10.1007/s11869-008-0020-0.

Liu, J., Clark, L. P., Bechle, M. J., Hajat, A., Kim, S. Y., Robinson, A. L., Sheppard, L., Szpiro, A. A., & Marshall, J. D. (2021). Disparities in Air Pollution Exposure in the United States by Race/Ethnicity and Income, 1990-2010. Environmental health perspectives, 129(12), 127005. https://doi.org/10.1289/EHP8584

Marinescu, P. J., Levin, E. J. T., Collins, D., Kreidenweis, S. M., and van den Heever, S. C. (2019). Quantifying aerosol size distributions and their temporal variability in the Southern Great Plains, USA, Atmos. Chem. Phys., 19, 11985–12006, https://doi.org/10.5194/acp-19-11985-2019

MPCA. https://www.pca.state.mn.us/air/assessing-urban-air-quality-project

MPCA. The air we breathe: The state of Minnesota's air quality 2019. https://www.pca.state.mn.us/sites/default/files/lraq-1sy19.pdf

Owoade, O.K., Abiodun, P.O., Omokungbe, O.R., Fawole, O.G., Olise, F.S., Popoola, O.O.M., Jones, R.L., Hopke, P.K. (2021). Spatial-temporal Variation and Local Source Identification of Air Pollutants in a Semi-urban Settlement in Nigeria Using Low-cost Sensors. Aerosol Air Qual. Res. 21, 200598. https://doi.org/10.4209/aaqr.200598

Pakbin, Hudda, N., Cheung, K. L., Moore, K. F., & Sioutas, C. (2010). Spatial and Temporal Variability of Coarse (PM10−2.5) Particulate Matter Concentrations in the Los Angeles Area. Aerosol Science and Technology, 44(7), 514–525. https://doi.org/10.1080/02786821003749509

Randle, A. (2016). The Challenges and Benefits of Local Air Quality Monitoring. Envirotech Online.

Schneider, P., Castell, N., Dauge, F.R., Vogt, M., Lahoz, W.A., Bartonova, A. (2018). A Network of Low-Cost Air Quality Sensors and Its Use for Mapping Urban Air Quality. In: Bordogna, G., Carrara, P. (eds) Mobile Information Systems Leveraging Volunteered Geographic Information for Earth Observation. Earth Systems Data and Models, vol 4. Springer, Cham. https://doi.org/10.1007/978-3-319-70878-2_5

Souza, A.P., Jan, B., Nawaz, F., Yousuf, M., Zai, Oliveira, S.S., Pavão, H.G., Fernandes, W.A., Ihaddadene, R., Ihaddadène, N., Oguntunde, P.E., Debora, A., & Santos (2019). Temporal variations of SO2 in an urban environment.

Tanzer, R., Malings, C., Hauryliuk, A., Subramanian, R., & Presto, A. A. (2019). Demonstration of a Low-Cost Multi-Pollutant Network to Quantify Intra-Urban Spatial Variations in Air Pollutant Source Impacts and to Evaluate Environmental Justice. International Journal of Environmental Research and Public Health, 16(14), 2523. https://doi.org/10.3390/ijerph16142523

Uria-Tellaetxe, I., & Carslaw, D. C. (2014). Conditional bivariate probability function for source identification. Environmental modelling & software, 59, 1-9. https://doi.org/10.1016/j.envsoft.2014.05.002

US EPA. (2003). Latest Findings on National Air Quality: 2002 Status and Trends. https://nepis.epa.gov/Exe/ZyPDF.cgi/P1003URM.PDF?Dockey=P1003URM.pdf

WHO. https://www.who.int/health-topics/air-pollution

VITA

Panik Mudiyanselage Varuni K. Abhayaratne was born in Colchester, UK in 1996 and was raised in Sri Lanka. Varuni graduated from Missouri University of Science and Technology in the fall of 2020 with a Bachelor of Science degree in Civil Engineering. She began her Master of Science program in Environmental Engineering at Missouri S&T in spring 2021. She received her Master of Science degree in Environmental Engineering from Missouri University of Science and Technology in May 2023.